ADVANCING EARTH AND SPACE SCIENCE

JGR Biogeosciences

RESEARCH ARTICLE
10.1029/2020JG005901

Key Points:

- The concentration and isotope signatures of dissolved inorganic carbon (DIC) varied considerably in four large rivers with different drainage basins in China
- The three largest Chinese rivers, the Yangtze, Yellow, and Pearl rivers, transport high amounts of millennium-aged DIC to the coastal seas
- The contributions of the different sources to riverine DIC were quantitatively calculated using dual isotopes and the MixSIAR model

Supporting Information:

- Supporting Information S1

Correspondence to:
X. Wang,
xuchenwang@ouc.edu.cn

Citation:
Shan, S., Luo, C., Qi, Y., Cai, W.-J, Sun, S., Fan, D., & Wang, X. (2021). Carbon isotopic and lithologic constraints on the sources and cycling of inorganic carbon in four large rivers in China: Yangtze, Yellow, Pearl, and Heilongjiang. *Journal of Geophysical Research: Biogeosciences*, *126*, e2020JG005901. https://doi.org/10.1029/2020JG005901

Received 11 JUN 2020
Accepted 22 JAN 2021

Author Contributions:

Conceptualization: Wei-Jun Cai, Xuchen Wang
Data curation: Di Fan
Formal analysis: Shuwen Sun, Di Fan
Funding acquisition: Xuchen Wang
Investigation: Sen Shan, Chunle Luo, Yuanzhi Qi, Xuchen Wang
Methodology: Sen Shan, Chunle Luo, Yuanzhi Qi, Shuwen Sun, Di Fan, Xuchen Wang
Resources: Wei-Jun Cai
Supervision: Xuchen Wang
Validation: Shuwen Sun
Writing – original draft: Sen Shan
Writing – review & editing: Wei-Jun Cai, Xuchen Wang

Carbon Isotopic and Lithologic Constraints on the Sources and Cycling of Inorganic Carbon in Four Large Rivers in China: Yangtze, Yellow, Pearl, and Heilongjiang

Sen Shan[1], Chunle Luo[1], Yuanzhi Qi[1], Wei-Jun Cai[2], Shuwen Sun[3], Di Fan[3], and Xuchen Wang[1,3]

[1]Key Laboratory of Marine Chemistry Theory and Technology/Center for Frontier Science of Deep Ocean and Earth System, Ocean University of China, Qingdao, China, [2]School of Marine Science and Policy, College of Earth, Ocean and Environment, University of Delaware, Newark, DE, USA, [3]Center for Isotope Geochemistry and Geochronology, Qingdao National Laboratory for Marine Science and Technology, Qingdao, China

Abstract Transport of terrigenous carbon by rivers has been affected extensively by climate change and anthropogenic activities in China over the last few decades. Here, we present results on carbon isotopes (^{13}C, ^{14}C) of dissolved and particulate inorganic carbon (DIC and PIC) and combined with major lithologic ions measured in the four largest rivers in China, namely, the Yangtze, Yellow, Pearl, and Heilongjiang rivers, to reveal the sources and transport of terrigenous inorganic carbon in the rivers. The DIC concentrations showed large variations in the four rivers and ranged from 253 to 3,122 μM. The Yangtze, Yellow and Pearl rivers transported high DIC contents that had low $\Delta^{14}C$ values of millennium-aged DIC and very old PIC; however, the Heilongjiang River presented a lower DIC concentration with much younger ^{14}C ages than the global average (1,100 μM). The strong correlations between the DIC isotope values and major lithological ions (Ca^{2+} and Mg^{2+}) suggest that chemical weathering played important but variable roles in controlling the production and fate of DIC in the rivers. Using dual isotopes and the MixSIAR model, we calculated that the chemical weathering of carbonate rocks contributed 95 ± 5% of the riverine DIC to the headwater of the Yangtze River while silicate rock weathering and riverine organic matter respiration contributed 62 ± 25% and 5 ± 5% of the DIC in the middle and lower reaches of the river, respectively. In contrast, chemical weathering of silicate rocks contributed the dominant fraction of DIC in the Yellow (55 ± 17%), Pearl (61 ± 20%) and Heilongjiang (83 ± 29%) rivers.

1. Introduction

Rivers are important pathways for the mobilization and transportation of large amounts of terrestrial carbon, both organic and inorganic, into the ocean (Cole et al., 2007; Ludwig and Probst, 1998 ; Meybeck, 1993; Milliman & Meade, 1983; Regnier et al., 2013). Globally, approximately 0.85 Gt (Gt = 1×10^{15} g) of terrestrial carbon consisting of 0.45 Gt of organic carbon (OC) and 0.40 Gt of IC is delivered to the coastal oceans annually by rivers (Bauer et al., 2013; Blair & Aller, 2012; Cai, 2011). For riverine IC, the majority is in the form of dissolved inorganic carbon (Cole et al., 2007; Gaillardet et al., 1999). Among the world's 25 largest rivers that carry approximately 42% of the terrestrial dissolved inorganic carbon (DIC), over 60% have high DIC concentrations >1,000 μM (Cai et al., 2008). The high concentrations and fluxes of DIC in large rivers thus represent a major transport pathway of atmospheric CO_2 and play an important role not only in carbon cycling but also in climate variability (Beaulieu et al., 2012; Dosseto, 2015 ; Kump et al., 2000).

Chemical weathering is a major process that regulates atmospheric CO_2 and controls DIC concentrations in rivers (Cai et al., 2008; Gaillardet et al., 1999; Goldsmith et al., 2010; Hartmann et al., 2009; Reeder et al., 1972). From a geological standpoint, the chemical weathering of carbonate and silicate rocks are the two most dominant processes that consume atmospheric CO_2 and contribute major ions (Na^+, K^+, Mg^{2+}, Ca^{2+}) and DIC to rivers (Berner et al., 1983; Meybeck, 1976, 1987). The chemical weathering of the most abundant rock minerals can be described by the following simplified reactions:

1. Carbonate rocks:

$$CaCO_3(\text{calcite}) + CO_2 + H_2O = Ca^{2+} + 2HCO_3^- \quad (1)$$

$$CaMg(CO_3)_2(\text{dolomite}) + 2CO_2 + 2H_2O = Ca^{2+} + Mg^{2+} + 4HCO_3^- \quad (2)$$

1. Silicate rocks

$$Mg_2SiO_4(\text{peridot}) + 4CO_2 + 4H_2O = 2Mg^{2+} + 4HCO_3^- + H_4SiO_4 \quad (3)$$

$$2NaAlSi_3O_3(\text{Sodium feldspar}) + 2CO_2 + 11H_2O = Al_2Si_2O_5(OH)_4 + 2Na^+ + 2HCO_3^- + 4H_4SiO_4 \quad (4)$$

During mineral dissolution, consumed atmospheric and soil CO_2 are transformed and dissolved as DIC (mainly as HCO_3^-) in rivers, which serves as an important pathway of carbon cycling on earth (Amiotte Suchet and Probst, 1995). The net CO_2 consumption by the weathering process is considered a major sink for atmospheric CO_2 (Raymo and Ruddiman, 1992; Richey, 2004). However, as shown by the above reactions, the two weathering processes differ in that carbonate weathering consumes 1 mol of atmospheric CO_2 and produces 2 mol of dissolved carbonate ions, with 1 mol from the dissolution of carbonate itself. In contrast, for silicate minerals containing no carbon, all of the consumed CO_2 is dissolved as carbonate ions during weathering. The global CO_2 consumption rate of weathering has been reported to be 21.9×10^{12} mol year^{-1}, with 12.3×10^{12} mol year^{-1} (approximately 60%) from carbonate weathering and 8.7×10^{12} mol year^{-1} (40%) from silicate weathering (Gaillardet et al., 1999; Meybeck, 1987; Moon et al., 2014). However, over geological time, silicate weathering could represent a major sink of CO_2 and the CO_2 consumed by carbonate weathering would eventually be counterbalanced by carbonate precipitation in marine environments.

The sources of riverine DIC vary significantly based on the drainage basin mineralogy and surrounding environment of different rivers. The DIC concentration in natural waters consists of bicarbonate anion (HCO_3^-), carbonate anion (CO_3^{2-}), and dissolved CO_2 (including carbonic acid and CO_{2aq}) in water-temperature- and pH-dependent chemical equilibrium. Under natural environmental conditions, HCO_3^- is the dominant component of DIC in rivers and oceans (Millero, 2013). Most studies on the sources of riverine DIC have been based on the determination of dissolved lithologic ions, such as Na^+, K^+, Mg^{2+}, and Ca^{2+}, which are derived from chemical weathering in rivers (Berner et al., 1983; Gaillardet et al., 1999; Goldsmith et al., 2010; Meybeck, 1987). For example, based on the measured riverine dissolved ion load and HCO_3^- concentrations, Gaillardet et al. (1999) calculated that the global consumption flux of CO_2 by rock chemical weathering was 0.288 Gt C year^{-1}, with 51% by carbonate weathering and 49% by silicate weathering, which are comparable to previously reported values (Berner et al., 1983; Holland, 1978; Meybeck, 1987). As a result, a large fraction of CO_2 consumed by rock weathering is dissolved as HCO_3^- and transported as DIC in rivers. For some rivers with less of a chemical load from rock weathering, organic matter (OM) decomposition has a considerable effect on riverine DIC because microbiol respiration of OM transfers OC to CO_2 and then a portion of the CO_2 is dissolved as HCO_3^- in the riverine DIC pool. Using radiocarbon measurements, Mayorga et al. (2005) found that after acidifying water samples collected from the Amazon River, the stripped CO_2 had relatively modern ^{14}C values (−17‰–98‰), indicating that CO_2 dissolved and outgassing from the Amazon River was derived from the respiration of recently fixed biomass OM. This finding is consistent with the report of Richey et al. (2002), who estimated that degradation of terrestrial OM contributes approximately 75% of the CO_2 found in the Amazon River basin. Because the partial pressure of CO_2 (pCO_2) measured in many large rivers, such as the Amazon (Richey et al., 2002) and Mississippi (Reiman & Xu, 2019), is supersaturated with respect to atmospheric CO_2, rivers could represent important sources of CO_2 to the atmosphere (Butman & Raymond, 2011; Raymond et al., 2013; Stets et al., 2017). In addition to chemical weathering and OM respiration, other sources contribute to riverine DIC, such as groundwater and anthropogenic inputs (Duvert et al., 2019; Wachniew, 2006; Zeng & Masiello, 2010). The contributions to riverine DIC from all these sources could also have strong seasonal variability and may largely depend on the geological and environmental settings of the river drainage basins.

Radiocarbon has been a useful tool for identifying not only the sources but also the cycling time of carbon in rivers (Mayorga et al., 2005; Raymond et al., 2007, 2013; Wang et al., 2016; Zeng & Masiello, 2010). This method overcomes the possible overlap of using stable carbon isotopes to identify DIC sources, such as carbonate dissolution and atmospheric CO_2. The majority of riverine DIC has been reported to present modern $\Delta^{14}C$ values (+2‰, $n = 209$) (Marwick et al., 2015), suggesting that the DIC in the rivers was derived from

Table 1
General Information on the Four Largest Rivers Studied in China

River	Length (km)[a]	Basin area ($\times 10^4$ km^2)[a]	Water discharge (km^{3}year^{-1})[b]
Yangtze	6,397	180	893
Yellow	5,464	79.5	29
Pearl	2,214	45.4	282
Heilongjiang[c]	3,474	89.1	117

[a]Data from Xu (2006). [b]Average discharge rates for the Yangtze, Yellow, and Pearl rivers over the last 50 years (1950–2015) from the Sediment *Bulletin of Chinese Rivers* (2018). Discharge rate for the Heilongjiang River was from Xu (2006). [c]Length of the Heilongjiang River indicates the length of the river in China.

present-day biomass degradation and silicate weathering consuming atmospheric CO_2 (Marwick et al., 2015; Raymond et al., 2013). This finding challenges the enduring geochemical belief that river DIC is largely controlled by chemical weathering of carbonate rocks (Berner et al., 1983; Holland, 1978; Meybeck, 1987).

Here, we present the first data set that combines carbon isotope (^{13}C and ^{14}C) and lithologic studies of the sources and fluxes of DIC in the four largest rivers in China: the Yangtze, Yellow, Pearl, and Heilongjiang rivers. In recent years, although the high riverine DIC concentrations in the Yangtze, Yellow, and Pearl rivers have been studied extensively (Cai et al., 2008; Z. Y. Liu et al., 2014; L. L. Wu et al., 2005; L. J. Zhang et al., 2014), the DIC sources have not been well traced. In addition to biomass- or atmospheric-derived CO_2, whether carbonate weathering or silicate weathering is the major process controlling DIC in rivers remains controversial. Some studies have reported that carbonate weathering is likely the major factor (>90%) affecting DIC in the Yangtze and Yellow Rivers (Gaillardet et al., 1999; J. Y. Li & Zhang, 2005; Moon et al., 2014; Z. L. Wang et al., 2007; Zhang et al., 1995), whereas other studies have shown that silicate weathering provides the most DIC in rivers (Chetelat et al., 2008; Wang et al., 2016; Wu et al., 2008a, 2008b). Our goal is to use carbon isotope (^{13}C, ^{14}C) measurements combined with lithologic results to quantitatively determine the sources of DIC as well as particulate inorganic carbon (PIC) in these rivers.

2. Methods

2.1. Study Area

The Yangtze (Changjiang), Yellow (Huanghe), Pearl (Zhujiang), and Heilongjiang Rivers are the four largest rivers in China, and together, they drain ~41% of China's continental land. General geographic information of the four rivers is summarized in Table 1, and their drainage basins are shown in Figure 1. As the largest river in China, the Yangtze River is also ranked the third longest river (6,397 km) in the world (Milliman and Meade, 1983). The Yangtze River originates in the Qinghai-Tibetan Plateau and drains the Yun-Gui Plateau, the Sichuan Basin, the Three-Gorges region and subtropical plains in central and eastern China, and it finally flows into the East China Sea (ECS), undergoing a 6,620 m elevation drop (Cai et al., 2008; J. S. Chen et al., 2002). The Yangtze River is divided into four basins: the headwater and the upper, middle, and lower reaches. The headwater region consists of water from the Tongtian (sites C1–C2) and Jinsha (sites C3–C5) rivers (the same river is given two names for different river lengths; Figure 1). The geo-environment in the river's upper (sites C6–C11) and middle (sites C12–C14) reaches mainly consists of evaporites and carbonate rocks (Cai et al., 2008; J. S. Chen et al., 2002). The lower reach (sites C15–C17) of the river flows through a densely populated eastern plain to the Yangtze River Estuary. The average water discharge rate of the Yangtze River is ~893 km^3 year^{-1} (average value from 1950 to 2015, Sediment Bulletin of Chinese Rivers, 2018), which provides approximately 90% of the freshwater input to the ECS annually (C. T. A. Chen et al., 2008).

The Yellow River is the second longest river in China, and it has a total flow length of 5,464 km from its headwater in the Qinghai-Tibetan Plateau to the river mouth. The Yellow River drains a basin area of 795,000 km^2 (Xu, 2006) before entering the western Bohai Sea (Figure 1). The drainage basin of the Yellow River encompasses a broad range of geological tectonic features, from very old metamorphic rocks to modern fluvial-lacustrine sediments, including carbonates and clastic rocks of Paleozoic to Mesozoic age (Cai et al., 2008; W. G. Liu et al., 2007; Zhang et al., 1995a 1995b). The most significant feature of the Yellow River is its middle reach (sites H5–H6), which flows through the Loess Plateau, one of the largest and thickest Quaternary loess deposits in the world (Hirshfield & Sui, 2011; W. G. Liu et al., 2007). Thus, despite its low discharge rate (29 km^3 year^{-1}, average value from 1950 to 2015, Sediment Bulletin of Chinese Rivers, 2018), the Yellow River was once ranked the most turbid river in the world (Milliman & Meade, 1983). In the last few decades, however, the Yellow River has been regulated largely by human activities, with over 200 large- and mid-sized dams and reservoirs built along the river basin, which have reduced the export of suspended sediment by 90% (Walling & Fang, 2003; Wang et al., 2016).

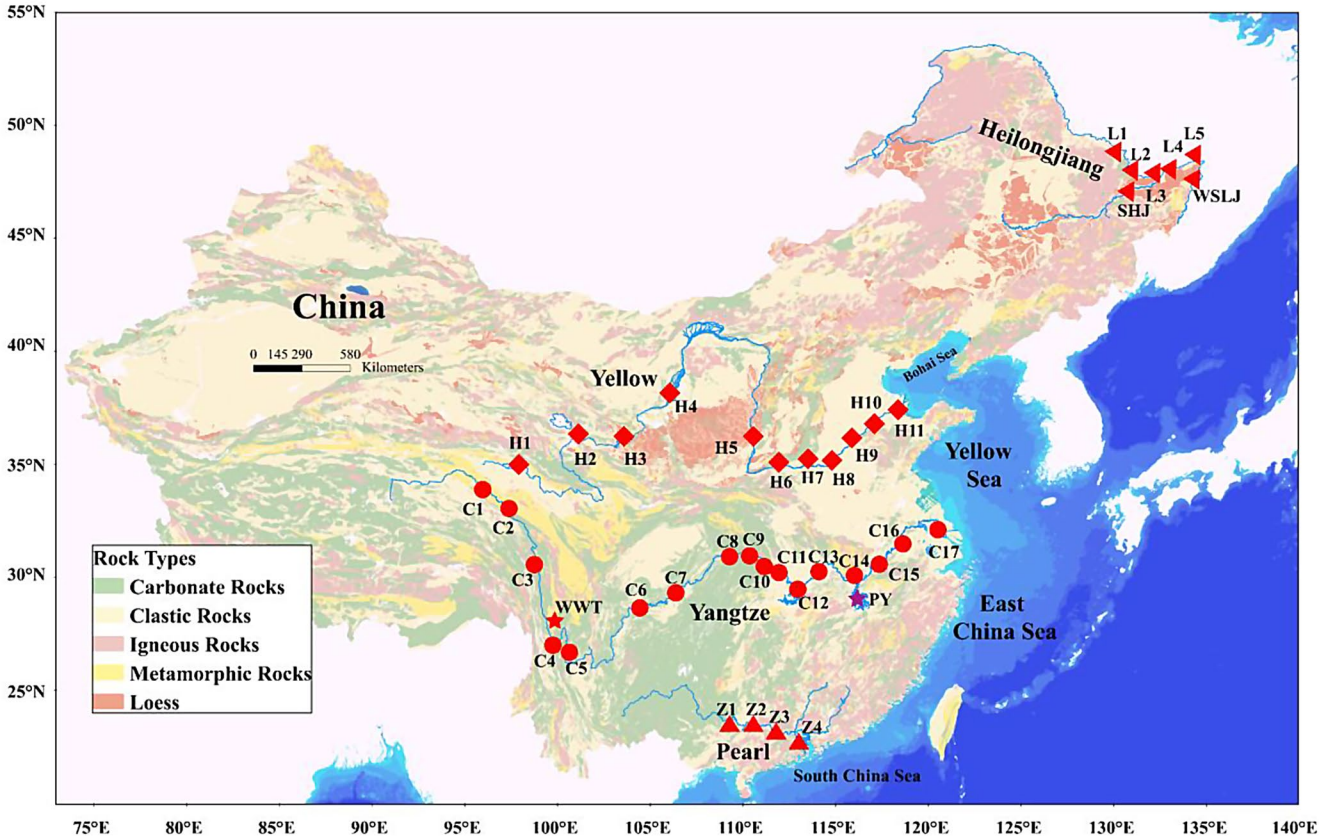

Figure 1. Geological map showing the drainage basin and sampling sites along the Yangtze River (● C1 to C17), Yellow River (◆ H1 to H11), Pearl River (▲ Z1 to Z4), and Heilongjiang River (◄ L1 to L5). Two sampling sites along the Yangtze River are listed: The White-Water Terrace (WWT, ★) in the upper basin and Poyang Lake (PY, ★) in the lower basin. For the Heilongjiang River, two samples were collected in the river's main tributaries: The Songhuajiang (SHJ, ◄) and Wusulijiang (WSLJ, ◄). The colors show the dominant rock type along the river basin.

The Pearl River is the third longest river (2,214 km) and ranked the second largest river in China in terms of its water discharge rate (282 km^3 $year^{-1}$; Table 1, Figure 1). The Pearl River originates in the northern Maxun Mountain region in Yunnan Province and drains a basin area of 454,000 km^2 in the south of China before entering the northern South China Sea (SCS; Cai et al., 2008; Xu, 2006). The lower reach of the Pearl River has three main tributaries, that is, the west river, north river, and east river, and these three rivers flow into the Pearl River Estuary. The west river is the main water flow source of the Pearl River (Figure 1).

The Heilongjiang River is in the far north of China, and it is shared as a boundary line between China and Russia (Figure 1). The Heilongjiang River is part of the Amur River flowing in China. The main stream of the Heilongjiang River originates in Inner Mongolia of China and has a total length of ~3,474 km (Xu, 2006). The Heilongjiang River basin consists of 49% sediments (6% of which are carbonates), 26% volcanics, 22% plutonics, and 3% metamorphics (Hartmann et al., 2012). In the lower reach of the Heilongjiang River, two major tributary rivers: Songhuajiang (SHJ) and Wusulijiang (WSLJ) flow into the river (Figure 1). Due to the long-frozen winter and remote location, the Heilongjiang River has been less influenced by human activities. Comprehensive studies on DIC in the Heilongjiang River have not been reported in the literature.

2.2. Sample Collection

Samples were collected from the headwater to the estuary of the Yangtze and Yellow rivers (Figure 1). A total of 11 stations were sampled along the Yellow River during May and June 2015, and 17 stations were sampled along the Yangtze River main streams from April to October 2016. The selection of the sampling sites was largely based on the sampling convenience and representative of different river flow lengths. In addition, for the Yangtze River basin, water from two special sites were collected. The first site was the

White-Water Terrace (WWT), which is a carbonate dissolution reference site located ~80 km east of the Yangtze River upper reach (Figure 1). Here, highly DIC-saturated water flows continually from a mountain spring and forms many small water pools and white carbonate deposition walls downhill (Figure S1). We also collected water samples from Poyang Lake (PY), which is the largest freshwater lake connected with the lower reach of the Yangtze River (Figure 1), and water from the lake flows into the river during the rainy season. Samples were collected at four sites in the middle to lower reaches of the Pearl River (Z1–Z4) in April 2018 (Figure 1). For the Heilongjiang River, samples at 7 sites (L1–L5 in the main stream and SHJ and WSLJ in the tributaries) (Figure 1) were collected in the river's lower reach in September 2017. Detailed information on the sampling sites in each river is provided in Table S1.

Water samples from each river site were collected from the main channel using small boats. Subsurface water (0.5–1.0 m) was collected using a precleaned stainless-steel bucket, and water from the lower part of the bucket was drained immediately into a narrow 100-mL borosilicate glass bottle with a ground-glass neck using precleaned silicone tubing. After overflowing approximately 100 mL of water from the full bottle, 50 μL of saturated $HgCl_2$ solution was added to the sample using a pipette and the bottle was capped tightly with a grease-coated ground-glass stopper. All sample bottles were secured with wide rubber bands to ensure a gas-tight seal (McNichol et al., 1994). Triplicate samples were collected for DIC concentration, total alkalinity (Alk) and isotope analyses. Suspended particles were collected by filtration of 4–5 L water through prebaked (550°C for 4 h) GF/F (0.7 μm) filters (Luo, 2017). Water samples for major lithologic ion measurements were collected at the same time by filtering river water through 0.2 μm polypropylene membrane filters. The samples were then acidified to pH <2 with 10% HCl, stored in polypropylene bottles and kept at room temperature. The river water temperature and pH values were measured on-site during sampling. The pH was measured using a METTLER TOLEDO FE 20 pH meter with precision of ±0.01. In addition, the temperature was measured using a THERMO TA-288 digital thermometer with precision of ±0.1°C.

2.3. Chemical Analyses (DIC, Alk, and Ions)

For the DIC concentration measurements, a 20 mL water sample was filtered with a 0.45 μm cellulose acetate membrane attached to a glass syringe in an N_2-filled bag and the DIC was measured using a Shimadzu TOC-L Analyzer equipped with an ASI-L autosampler with total inorganic carbon (IC) mode (X. C. Wang et al., 2016). A DIC standard solution was prepared using reagent-grade sodium carbonate and sodium bicarbonate dissolved in DIC-free Milli-Q water. The instrument blank and DIC values were checked against Certified Reference Materials (CRMs) provided by Dr. A.G. Dickson of the Scripps Institute of Oceanography, University of California San Diego. The average blank value associated with DIC measurements was <2.0 μmol, and the analytic precision on triplicate injections was ±2% or better. The total Alk was measured using the 848 Titrino Plus Automatic Potentiometric Titration method based on Gran titration (Gran, 1950). The precision of the method was ±0.1% based on replicate analyses for DIC standards. All measurements were made within 5 days after sample collection.

Based on the measured DIC, pH, and temperature, we calculated the CO_2 partial pressure pCO_2 values using the CO2SYS program (Lewis et al., 1998) by setting salinity = 0 for freshwater and using K1 and K2 values from Millero (1979). Similarly, the HCO_3^- concentrations were calculated based on DIC, pH and temperature. Due to the low Alk (<1,000 μeq L^{-1}) values measured in the Heilongjiang River, the calculated partial pressure pCO_2 was corrected for errors from organic alkalinity and pH measurements in low ionic strength freshwaters according to S. Liu et al. (2020).

Concentrations of the major cations (Ca^{2+} and Mg^{2+}) were measured by inductively coupled plasma atomic emission spectrometry (ICP-AES, iCAP 6300, Thermo, UK) using 2% HCl solution as a blank. The analytical precision was ±2% for both Ca^{2+} and Mg^{2+}. Unfortunately, other ions such as Si, K, and Na were not measured in this work.

2.4. Carbon Isotope Measurement

Carbon isotopes (^{13}C and ^{14}C) were measured for both DIC and PIC. For DIC, we used a modified DIC extraction method (Ge et al., 2016; Wang et al., 2016) based on McNichol et al. (1994). Briefly, in an N_2-filled bag, 50 mL

of each river water sample was filtered using a syringe-type 0.45 μm cellulose acetate membrane and injected through a rubber septum-sealed tube into a preevacuated 100-mL borosilicate glass bottle connected to a stripping probe by a ground-glass joint. Then, 1.0 mL 85% H_3PO_4 solution was injected into the bottle to acidify DIC to pH ≤ 2. The glass bottle was placed in a 70°C hot water bath for 30 min and shaken several times by hand. At pH ≤ 2, all forms of DIC (carbonate, bicarbonate, and CO_2) dissolved in water will become CO_2. The glass bottle was removed from the hot water bath, cooled for 5 min, and then attached at the top to a vacuum line. All CO_2 generated from DIC was collected cryogenically in the liquid nitrogen trap. After measuring the volume of CO_2 (for the extraction efficiency calculation), the CO_2 was flame-sealed inside 6 mm OD Pyrex tubes for the ^{13}C and ^{14}C analyses. The extraction efficiency of the method was >97% for all samples as determined via comparisons with the DIC concentration. Blanks associated with the DIC extraction method were trivial (~2 μg C). For the PIC isotopic measurement, particles collected on the GF/F filters were placed in a specially designed reaction tube for acidification. PIC was acidified with 85% H_3PO_4 in the evacuated tube, and the CO_2 released from the PIC was collected and purified cryogenically on a vacuum line. After the CO_2 volume was measured, the CO_2 was flame-sealed inside 6 mm OD Pyrex tubes for the ^{13}C and ^{14}C analyses (Wang et al., 2016).

The isotopic ($\delta^{13}C$ and $\Delta^{14}C$) values of the Yangtze and Yellow river samples were measured in the National Ocean Science Accelerator Mass Spectrometry (NOSAMS) facility at Woods Hole Oceanographic Institution (WHOI), USA, and samples from the Pearl and Heilongjiang rivers were analyzed in the Center for Isotope Geochemistry and Geochronology (CIGG) at the Qingdao National Laboratory for Marine Science and Technology (QNLM) in Qingdao, China. A small split of CO_2 was measured for $\delta^{13}C$ using a dual-inlet Thermo 253 Plus Isotope Ratio Mass Spectrometer (IRMS) at the CIGG. Values of $\delta^{13}C$ were reported in ‰ relative to the IAEA carbonate standards, and the analytic deviation was <0.2‰ ($n = 10$). The sample ^{14}C was measured by accelerator mass spectrometry (AMS) after graphitization of CO_2. The $\Delta^{14}C$ values were reported as the modern fraction based on modern reference material (OX-I or OX-II). Because all our sample sizes ranged from 600 to 1,000 μg C for the DIC and PIC $\Delta^{14}C$ measurements, the replication of samples was >96%; moreover, the analytical precision was generally <5‰. Conventional radiocarbon ages (years before present) were calculated based on the equation of Stuiver and Polach (1977):

$$\Delta^{14}\mathrm{C}(‰) = \left[F_m \times e^{\lambda(1950 - Yc)} - 1\right] \times 1{,}000 \tag{5}$$

$$^{14}\mathrm{C\ Age} = -8{,}033 \ln(F_m) \tag{6}$$

where F_m is the modern ^{14}C fraction; $\lambda = 1/8{,}267$; and Yc is the year of sample collection.

2.5. Quantification of the Potential Sources of Riverine DIC

To quantify and compare the contributions of different sources of riverine DIC in the four large rivers in China, we used dual isotopes ($\delta^{13}C$ and $\Delta^{14}C$) and the MixSIAR model. The MixSIAR model is a Bayesian mixing model with improvement upon simpler linear mixing models by explicitly taking into account uncertainty in source values, categorical and continuous covariates (Stock & Semmens, 2016). The model can be used for ^{13}C and ^{14}C analyses to determine the carbon sources (Schuur et al., 2016). The riverine DIC was considered to be in chemical equilibrium, and a mixture was derived from four potential sources as follows: (1) DIC produced from the chemical weathering of rocks consuming atmospheric CO_2, (2) DIC produced from the chemical weathering of rocks consuming soil CO_2, (3) carbonate dissolution to DIC during weathering, and (4) DIC produced from OM respiration in the river. For the model calculation, the following equations were set:

$$\delta^{13}\mathrm{C}_{\mathrm{sample}} = f_{\mathrm{atm}}\delta^{13}\mathrm{C}_{\mathrm{atm}} + f_{\mathrm{soil}}\delta^{13}\mathrm{C}_{\mathrm{soil}} + f_{\mathrm{carb}}\delta^{13}\mathrm{C}_{\mathrm{carb}} + f_{\mathrm{om}}\delta^{13}\mathrm{C}_{\mathrm{om}} \tag{7}$$

$$\Delta^{14}\mathrm{C}_{\mathrm{sample}} = f_{\mathrm{atm}}\Delta^{14}\mathrm{C}_{\mathrm{atm}} + f_{\mathrm{soil}}\Delta^{14}\mathrm{C}_{\mathrm{soil}} + f_{\mathrm{carb}}\Delta^{14}\mathrm{C}_{\mathrm{carb}} + f_{\mathrm{om}}\Delta^{14}\mathrm{C}_{\mathrm{om}} \tag{8}$$

$$f_{\mathrm{atm}} + f_{\mathrm{soil}} + f_{\mathrm{carb}} + f_{\mathrm{om}} = 1 \tag{9}$$

Table 2
Carbon Isotopic Values of Potential DIC Sources in the Yangtze, Yellow, Pearl and Heilongjiang Rivers

Source	$\delta^{13}C$ (‰) Range	$\delta^{13}C$ (‰) Mean	$\Delta^{14}C$ (‰) Range	$\Delta^{14}C$ (‰) Mean	Reference
			Atmospheric CO_2		
	−6.3 to 0		−3.2	35	Ishikawa et al. (2015); Levin et al. (2010)
			Carbonate dissolution[a]		
	−2.2 to 1.1	−0.5	−964 to −872	−918	This study
			Organic matter respiration[b]		
Yangtze	−27.5 to −22.9	−25.2	−401 to −97	−249	Qi (2019)
Yellow	−28.8 to −23.1	−26	−613 to −58	−335	Xue et al. (2017)
Pearl	−31.2 to −26.7	−29	−270 to −124	−197	Qi (2019)
Heilongjiang	−31.4 to −26.2	−28.8	−204 to −52	−76	Qi (2019)
			Soil CO_2[c]		
Yangtze	−26 to −21	−23.5	−230 to −100	−165	Qi (2019); Zeng et al. (2011) and Y. Wu et al., (2007)
	−26 to −21	−23.5	28 to 42	35	
Yellow	−26 to −20	−23	−230 to −100	−165	Xue et al. (2017); Tao et al. (2016) and Zeng et al. (2011)
	−26 to −20	−23	28 to 42	35	
Pearl	−31 to −21	−26	−230 to −100	−165	Qi (2019); Yu et al. (2010) and Zeng et al. (2011)
	−31 to −21	−26	28 to 170	35	
Heilongjiang	−22 to −15	−18.5	−230 to −100	−165	Tu et al. (2018) and Zeng et al. (2011)
	−22 to −15	−18.5	28 to 42	35	

[a]Carbonate rock dissolution values were based on the results of PIC. [b]Isotope values of riverine OM respiration were based on the DOC and POC results in the four rivers. [c]Soil CO_2 was derived from respiration of terrestrial OM. The $\delta^{13}C$ of soil CO_2 was between −26‰ and −18‰ in the C_3 dominated area. The $\delta^{13}C$ ranges of the soil CO_2 were based on the different river basins and consider the fraction of CO_2 in H_2CO_3 and HCO_3^-, which could also represent the groundwater DIC signature. The $\Delta^{14}C$ of young soil was equivalent to atmospheric CO_2. The $\Delta^{14}C$ of old soil is the ^{14}C value from aged soil OM respiration, and it is also influenced by wastewater.

where f_{atm}, f_{soil}, f_{carb}, and f_{om} are the contribution fractions of the four potential DIC sources, namely, atmospheric CO_2 (f_{atm}), soil CO_2 (f_{soil}), dissolution of carbonate (f_{carb}), and respiration of OM (f_{om}), respectively; and $\delta^{13}C_{sample}$ and $\Delta^{14}C_{sample}$ are the measured isotopic values for the samples. The isotopic values assigned to each source end-member were expressed as $\delta^{13}C_{atm,}$ $\delta^{13}C_{soil,}$ $\delta^{13}C_{carb}$, and $\delta^{13}C_{om}$ and $\Delta^{14}C_{atm}$, $\Delta^{14}C_{soil}$, $\Delta^{14}C_{carb}$, and $\Delta^{14}C_{om}$, as listed in Table 2. In our calculation, we also defined the following:

$$F_{carb} = 2f_{carb} \tag{10}$$

$$F_{sili} = f_{atm} + f_{soil} - f_{carb} \tag{11}$$

$$f_{soil} = f_{soil-young} + f_{soil-old} \tag{12}$$

where F_{carb} is the total contribution to the riverine DIC from the chemical weathering of carbonate rocks (1/2 from carbonate dissolution +1/2 from the consumption of atmospheric and soil CO_2) and F_{sili} is the contribution of chemical weathering from silicate rocks consuming CO_2. Soil CO_2 (f_{soil}) was divided into CO_2 derived from young OM and preaged OM. The model calculation was based on the R package (2019) MixSIAR GUI (graphical user interface) program (Stock & Semmens, 2016).

3. Results

3.1. Distributions of DIC, Alk, pCO_2, Ca^{2+}, and Mg^{2+}

The concentrations of DIC, Ca^{2+}, and Mg^{2+} measured for the four rivers are provided in Table 3. The DIC concentrations showed large variations in the four rivers ranging from 253 to 3,122 μM. As plotted in Figure 2a, the Yangtze River headwater (C1–C4) had high DIC concentrations (2,846 ± 49 μM at C1), which decreased downstream to site C6 and then increased (C7–C11). The DIC concentrations in the middle (C12–C14, 1,749 ± 188 μM) and lower reaches (C15–C16, 1,585 ± 98 μM) of the Yangtze River were relatively lower than those in the headwater and upstream (Figure 2a). For the carbonate reference site WWT, the DIC concentration was very high at 16,198 ± 492 μM (Table 3). In comparison, the DIC concentration in the fresh lake of Poyang (PY) was much lower (387 ± 10 μM). The DIC concentrations in the Yellow River were the highest among the four rivers and ranged from 2,398 to 3,122 μM, with an average of 2,941 ± 206 μM (Table 3). The DIC along the Yellow River exhibited relatively constant distributions except at site H5 (Figure 2a). The DIC concentrations in the Pearl River ranged from 1,544 to 2,273 μM and decreased from the midstream site (Z1) to the lower reach (Z4; Figure 2a). Among the four rivers, the Heilongjiang River had the lowest DIC concentrations, with values ranging from 253 to 895 μM (average 448 ± 204 μM). The DIC concentration in the tributary SHJ was higher (895 μM) than that in the main streams of the Heilongjiang and WSLJ (Figure 2a). The calculations indicated that HCO_3^- was the dominant form of DIC and accounted for 95%, 97%, 90%, and 87% of the DIC in the Yangtze, Yellow, Pearl and Heilongjiang rivers, respectively. The measured total Alk ranged from 354 to 3,220 μeq/L (Table 3) and had very similar distributions as the DIC in the four rivers (Figure 2a).

The calculated partial pressure (pCO_2) of dissolved CO_2 in the rivers also varied widely, ranging from 384 to 10,803 μatm, with an average value of 1,834 ± 1,560 μatm in the Yangtze River, 1,555 ± 1,050 μatm in the Yellow River, 8,974 ± 1,391 μatm in the Pearl River and 1,322 ± 388 μatm in the Heilongjiang River (Table 3). The pCO_2 was lower (384–426 μatm) in the headwater (C1–C3), increased along the river, and remained relatively constant in the upper and middle reaches (C7–C13) in the Yangtze River, and it ranged from 587 to 4,104 μatm in the Yellow River and was higher in the upstream and relatively lower and constant in the middle and lower reaches (Figure 2b). The Pearl River had the highest pCO_2 values, which decreased along the river. The pCO_2 values were lower and constant in the main stream of the Heilongjiang River (537–780 μatm) and higher in the two tributaries, SHJ (1,667 μatm) and WSLJ (1,186 μatm). The four rivers were all supersaturated with pCO_2 with respect to atmospheric CO_2 (~400 μatm) except in the headwater of the Yangtze River (Figure 2b).

The concentration and distributions of Ca^{2+} and Mg^{2+} in the four rivers also showed large variations (Table 3). In the Yangtze River, the concentrations of Ca^{2+} ranged from 633 to 1,542 μM and were much higher than those of Mg^{2+} (178–1,056 μM). The concentrations of both Ca^{2+} and Mg^{2+} decreased from the headwater to downstream sites (Figure 2c). Site WWT again had the highest Ca^{2+} (9,248 μM) and Mg^{2+} (99,861 μM) concentrations (Table 3, not plotted in Figure 2c), and PY Lake had the lowest Ca^{2+} (216 μM) and Mg^{2+} (65 μM) concentrations (Table 3, Figure 2c). In the Yellow River, the Ca^{2+} and Mg^{2+} concentrations ranged from 327 to 1,528 μM and 267 to 1,250 μM, respectively, and exhibited different distribution patterns along the river, with lower values in the headwater and higher values downstream (Figure 2c). The concentration of Ca^{2+} was higher than that of Mg^{2+} in the upstream sites (except for H1) but lower than that of Mg^{2+} in the middle and downstream sites (except for H7; Figure 2c). In the Pearl River, the concentration of Ca^{2+} (average 1,193 ± 60 μM) was much higher than that of Mg^{2+} (average 309 ± 30 μM) and exhibited more constant distributions in the river (Figure 2c). In comparison, the concentrations of both Ca^{2+} and Mg^{2+} were lowest in the Heilongjiang River, with averages of 287 ± 105 μM and 119 ± 53 μM, respectively (Figure 2c).

3.2. Isotopic Compositions

The values of $\delta^{13}C$ and $\Delta^{14}C$ measured for the DIC and PIC in the four rivers are summarized in Table 4 and plotted in Figure 3. For the Yangtze River, the DIC $\delta^{13}C$ values ranged from −1.4‰ to −10.2‰ and were higher in the headwater (−1.4 to −4.6‰) and decreased toward downstream sites (−8.4 to −9.4‰) (Figure 3a). For DIC, the WWT site had the highest $\delta^{13}C$ value (−1.3‰) and PY Lake had the lowest $\delta^{13}C$ value (−11.3‰), whereas for PIC, the $\delta^{13}C$ values in the Yangtze River were higher than those of DIC and ranged from −2.2‰ to 1.1‰. The PIC in the four headwater sites (C1–C4) had high positive $\delta^{13}C$ values (0.3–1.1‰; Figure 3a).

Table 3
Concentration of DIC, Alk, HCO_3^-, Ca^{2+}, Mg^{2+} and pCO_2 in the Yangtze, Yellow, Pearl, and Heilongjiang Rivers

River	Sample ID	Ca^{2+} μM	Mg^{2+} μM	DIC μM	Alk μeq/L	HCO_3^- μM	pCO_2 μatm
				Yangtze River			
Tongtian	C1	1,542	1,056	2,846 ± 49	2,771 ± 36	2,787	405
	C2	1,481	882	2,766 ± 51	2,803 ± 20	2,708	426
	Mean	**1,512 ± 31**	**969 ± 87**	**2,806 ± 40**	**2,787 ± 16**	**2,748 ± 39**	**416 ± 10**
Jinsha	C3	1,386	800	2,687 ± 16		2,629	384
	C4	1,079	647	2,375 ± 57	2,257 ± 8	2,282	2047
	C5			2022 ± 28	1865 ± 25	1892	2,980
	Mean	**1,233 ± 153**	**723 ± 77**	**2,361 ± 272**	**2,188 ± 241**	**2,268 ± 301**	**1803 ± 1,073**
Upstream	C6	803	367	1844 ± 23	1,695 ± 22	1708	3,138
	C7	878	382	2,190 ± 36	2,190 ± 58	2,137	991
	C8	1,135	464	2,375 ± 11	2,299 ± 17	2,318	1,036
	C9			2,360 ± 10	2,361 ± 47	2,312	682
	C10			2,427 ± 20	2,347 ± 10	2,364	1,114
	C11			2,359 ± 35	2,220 ± 16	2,299	1,076
	Mean	**939 ± 142**	**404 ± 43**	**2,259 ± 200**	**2,185 ± 228**	**2,190 ± 227**	**1,340 ± 816**
Midstream	C12	633	178	1,483 ± 9	1,554 ± 46	1,422	1,347
	C13	928	322	1893 ± 13	1965 ± 30	1833	1,257
	C14	918	299	1871 ± 10	1877 ± 11	1,260	4,870
	Mean	**826 ± 137**	**266 ± 63**	**1749 ± 188**	**1799 ± 177**	**1,505 ± 241**	**2,491 ± 1,682**
Downstream	C15	729	255	1,487 ± 10	1,574 ± 10	1,212	5,862
	C16	779	276	1,682 ± 6	1,622 ± 12	1,598	1723
	Mean	**754 ± 25**	**266 ± 11**	**1,585 ± 98**	**1,585 ± 98**	**1,405 ± 193**	**3,792 ± 2069**
Mean		**995 ± 254**	**481 ± 256**	**2,167 ± 416**	**2,115 ± 384**	**2048 ± 487**	**1834 ± 1,560**
	PY	216	65	387 ± 10	803 ± 15	221	3,565
	WWT	9,248	99,861	16,198 ± 492			
				Yellow River			
Upstream	H1	327	411	3,036 ± 12	3,215 ± 15	2,944	1,276
	H2	480	267	2,715 ± 55	2,910 ± 28	2,596	2073
	H3	973	505	2,843 ± 31	3,066 ± 63	2,741	2,163
	H4	918	677	3,122 ± 20	3,220 ± 56	2,954	4,104
	Mean	**674 ± 277**	**465 ± 149**	**2,929 ± 160**	**3,103 ± 127**	**2,809 ± 149**	**2,403 ± 1,040**
Midstream	H5	820	1,035	2,398 ± 48	2,857 ± 29	2,325	1850
	H6	750	1,182	3,111 ± 19	3,206 ± 24	3,049	905
	Mean	**785 ± 35**	**1,109 ± 74**	**2,755 ± 356**	**3,032 ± 175**	**2,687 ± 362**	**1,378 ± 472**
Downstream	H7	1,528	1,250	3,069 ± 32	3,162 ± 26	3,006	787
	H8	815	1,148	3,058 ± 22	3,182 ± 13	2,994	710
	H9	895	1,150	3,003 ± 46	3,120 ± 26	2,941	632
	H10	957	1,165	2,988 ± 23	3,170 ± 27	2,922	587
	H11	1,045	1,160	3,006 ± 30	3,136 ± 34	2,927	2021
	Mean	**1,048 ± 252**	**1,175 ± 38**	**3,025 ± 32**	**3,154 ± 43**	**2,958 ± 35**	**947 ± 541**
Mean		**864 ± 294**	**905 ± 347**	**2,941 ± 206**	**3,113 ± 130**	**2,855 ± 218**	**1,555 ± 1,050**

Table 3
Continued

River	Sample ID	Ca^{2+} μM	Mg^{2+} μM	DIC μM	Alk μeq/L	HCO_3^- μM	pCO_2 μatm
Pearl River	Z1	1,272	351	2,273 ± 10	2,759 ± 9	1856	10,803
	Z2	1,128	281	2082 ± 15	2,529 ± 1	1753	8,686
	Z3	1,178	294	1998 ± 25	2,352 ± 12	1723	7,433
	Z4			1,544 ± 6	1749 ± 38		
Mean		**1,193 ± 60**	**309 ± 30**	**1974 ± 268**	**2,347 ± 374**	**1777 ± 57**	**8,974 ± 1,391**
Heilongjiang River	L1	195	85	305 ± 1	430 ± 5	249	707 ± 51
	L2	187	53	285 ± 3	432 ± 23	235	662 ± 49
	L3			253 ± 1	354 ± 21	210	537 ± 40
	L4	300	129	514 ± 9	684 ± 22	467	680 ± 44
	L5	274	119	414 ± 6	575 ± 14	361	781 ± 53
	SHJ	478	210	895 ± 3	1,302 ± 8	806	1,667 ± 94
	WSLJ			472 ± 3	709 ± 4	398	1,186 ± 78
Mean		**287 ± 105**	**119 ± 53**	**448 ± 204**	**641 ± 297**	**389 ± 191**	**889 ± 399**

Note: Space left blanks are not measured. DIC, dissolved inorganic carbon; PIC, particulate inorganic carbon; PY, Poyang Lake; SHJ, Songhuajiang; WSLJ, Wusulijiang; WWT, White-Water Terrace.

The values of $\delta^{13}C$ for both DIC and PIC showed less variation in the Yellow River and ranged from −7.0‰ to −2.2‰ for DIC and from −3.8‰ to −2.2‰ for PIC. The DIC $\delta^{13}C$ values in the downstream of the Pearl River were less variable and ranged from −9.1‰ to −9.7‰, and the PIC $\delta^{13}C$ values (only one site) were much higher (−2.0‰) than that of DIC. The DIC $\delta^{13}C$ values in the Heilongjiang River main stream were low (−11.3 ± 2.0‰) and slightly higher at sites L4, SHJ and WSLJ. No PIC was collected in the Heilongjiang River.

The $\Delta^{14}C$ values of DIC and PIC also showed large variations (Table 4). In the Yangtze River, the DIC $\Delta^{14}C$ ranged from −125‰ to −455‰ and the values increased from the headwater to downstream and remained constant in the middle and lower reaches (Figure 3b). The DIC $\Delta^{14}C$ values in the headwater of Tongtian (C1–C2, −444 ± 11‰) and Jinsha (C3–C5, −355 ± 37‰) were significantly lower than those at other sites. The calculated ^{14}C ages indicated that the DIC in the headwater was much older (4,655 ± 165 years) than that in the lower reaches (1,260 ± 70 years) of the Yangtze River. The DIC ^{14}C age was the oldest (22,400 years) at the WWT site and the youngest at the PY Lake site (615 years; Figure 3b). In comparison, the $\Delta^{14}C$ values of PIC were much lower than those of DIC in the Yangtze River and ranged from −756‰ to −915‰; the corresponding ^{14}C ages were 11,250 to 19,800 years, which was over 10,000 years older than the DIC ages (Figure 3b). The DIC $\Delta^{14}C$ in the Yellow River ranged from −138‰ to −231‰ and slightly increased from the headwater to the middle stream and remained steady (Figure 3b). Similar to the PIC in the Yangtze River, the Yellow River PIC also had very depleted $\Delta^{14}C$ values (average −937 ± 34‰) and was much older (average 23,020 ± 3,699 years) than the average DIC age (1,358 ± 285 years; Figure 3b). In the Pearl River, the DIC had relatively constant $\Delta^{14}C$ values (−137 ± 8‰) and ^{14}C ages (1,115 ± 76 years). Again, the only PIC in the Pearl River was much older (10,570 years) than the DIC in the Pearl River. In comparison, the DIC in the Heilongjiang River had relatively modern $\Delta^{14}C$ values that ranged from −28‰ to −110‰, which corresponded to ^{14}C ages of 165–865 years (Figure 3b).

4. Discussion

4.1. Variations of DIC in the Rivers

The concentrations and distributions of DIC, total Alk, and cations (Ca^{2+} and Mg^{2+}) in the four large rivers in China showed wide variations. In general, the Yellow River had the highest DIC concentrations (average 2,941 ± 206 μM) and Alk (3,113 ± 130 μeq/L), followed by the Yangtze (2,167 ± 416 μM, 2,115 ± 384 μeq/L), Pearl (1,974 ± 268 μM, 2,347 ± 374 μeq/L), and Heilongjiang (448 ± 204 μM, 641 ± 297 μeq/L) rivers

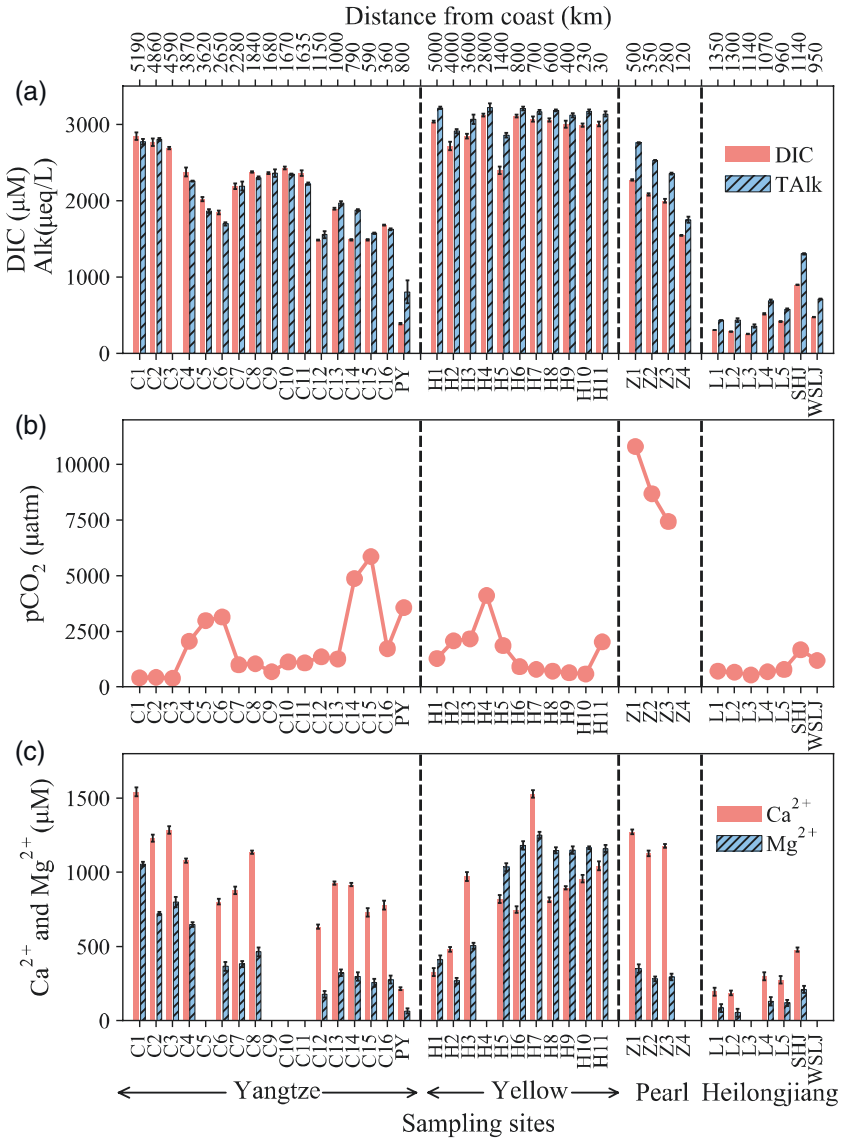

Figure 2. Concentrations of (a) DIC and Alk, (b) calculated pCO_2, and (c) measured Ca^{2+} and Mg^{2+} for the four rivers. The distance is measured from the river mouth. Error bars represent the range of duplicate measurements. Alk, alkalinity; DIC, dissolved inorganic carbon; pCO_2, partial pressure of CO_2.

(Figure 2a and 2c). We compared these DIC concentrations with that of the 12 largest rivers in the world in terms of the discharge rates. As shown in Figure 4a, the concentrations of DIC carried by the Yellow, Yangtze, and Pearl rivers are among the highest in the large rivers worldwide (Cai et al., 2008; Gaillardet et al., 1999; Goldsmith et al., 2010). The concentration of DIC identified in the Heilongjiang River was comparable to that in the Congo and Orinoco rivers (Figure 4a). These observed differences in the DIC distribution in the four studied rivers could be controlled by many factors, such as differences in the drainage basin environmental settings, mineral coverage differences, climate variability and anthropogenic influences (Cai et al., 2008; Zhang et al., 2013, 2014). Additionally, some of the variations could be related to the seasonal variations because we conducted our field sampling at different times and seasons for each river.

The Yangtze and Pearl rivers flow through a subtropical climate region, and the concentrations of DIC in these two rivers are comparable. Thus, the DIC in the two rivers are likely controlled by the similar processes. The upper streams of both the Yangtze and Pearl rivers drain basement rocks that consist of evaporites and continental deposits abundant in carbonates (Cai et al., 2008; J. S. Chen et al., 2002; S. Y. Li et al., 2011). The

Table 4
Isotopic Values of DIC, PIC in the Yangtze, Yellow, Pearl, and Heilongjiang Rivers

River	Sample ID	DIC			PIC		
		$\delta^{13}C$ (‰)	$\Delta^{14}C$ (‰)	Age (year)	$\delta^{13}C$ (‰)	$\Delta^{14}C$ (‰)	Age (year)
				Yangtze River			
Tongtian	C1	−1.4	−455	4,820	0.5	−757	11,300
	C2	−2.0	−433	4,490	1.1	−781	12,150
	Mean	**−1.7 ± 0.3**	**−444 ± 11**	**4,655 ± 165**	**0.8 ± 0.3**	**−769 ± 12**	**11,725 ± 425**
Jinsha	C3	−2.8	−402	4,070	0.4	−756	11,250
	C4	−3.0	−354	3,450	0.3	−766	11,600
	C5	−4.6	−310	2,920	−0.6	−805	13,050
	Mean	**−3.4 ± 0.8**	**−355 ± 37**	**3,480 ± 470**	**0.0 ± 0.4**	**−776 ± 21**	**11,967 ± 779**
Upstream	C6	−6.4	−224	1,980			
	C7	−6.3	−223	1,960	−0.8	−915	19,800
	C8	−7.2	−194	1,670			
	C9	−7.2	−175	1,480			
	C10	−7.7	−185	1,580			
	C11	−7.7	−179	1,530			
	Mean	**−7.1 ± 0.6**	**−197 ± 20**	**1,700 ± 199**	**−0.8**	**−915**	**19,800**
Midstream	C12	−10.2	−125	1,010			
	C13	−9.2	−148	1,220	−2.2	−786	12,350
	C14	−8.8	−150	1,250			
	Mean	**−9.4 ± 0.6**	**−141 ± 11**	**1,160 ± 107**	**−2.2**	**−786**	**12,350**
Downstream	C15	−8.6	−161	1,350			
	C16	−8.5	−143	1,180	−0.6	−894	17,950
	C17	−8.2	−151	1,250			
	Mean	**−8.4 ± 0.2**	**−152 ± 8**	**1,260 ± 70**	**−0.6**	**−894**	**17,950**
Mean		**−6.5 ± 2.6**	**−236 ± 107**	**2,189 ± 1,222**	**−0.2 ± 1.0**	**−807 ± 58**	**13,681 ± 3,084**
	PY	−11.3	−81	615			
	WWT	−1.3	−939	22,400			
				Yellow River			
Upstream	H1	−2.2					
	H2	−6.5	−231	2,050	−2.6	−964	26,500
	H3	−7.0	−192	1,650			
	H4				−2.2	−959	25,500
	Mean	**−5.2 ± 2.2**	**−212 ± 20**	**1850 ± 200**	**−2.4 ± 0.2**	**−961 ± 2**	**26,000 ± 500**
Midstream	H5	−2.3	−155	1,290			
	H6	−5.7	−144	1,190			
	TG				−3.8	−956	25,100
	ZW				−2.3	−932	21,600
	Mean	**−4.0 ± 1.7**	**−149 ± 5**	**1,240 ± 50**	**−3.1 ± 0.8**	**−944 ± 12**	**23,350 ± 1750**

Table 4
Continued

River	Sample ID	DIC			PIC		
		$\delta^{13}C$ (‰)	$\Delta^{14}C$ (‰)	Age (year)	$\delta^{13}C$ (‰)	$\Delta^{14}C$ (‰)	Age (year)
Downstream	H7	−6.2	−153	1,270			
	H8	−6.2	−152	1,260			
	H9	−5.6	−138	1,130			
	H10	−5.4	−138	1,130			
	H11	−6.2	−151	1,250	−4.4	−872	16,400
	Mean	**−5.9 ± 0.3**	**−146 ± 7**	**1,208 ± 64**	**−4.4**	**−872**	**16,400**
Mean		**−5.3 ± 1.6**	**−162 ± 29**	**1,358 ± 285**	**−3.1 ± 0.9**	**−937 ± 34**	**23,020 ± 3,699**
Pearl River	Z1	−9.7	−145	1,190	−2.0	−734	10,570
	Z2	−9.4	−138	1,120			
	Z3	−9.1	−141	1,160			
	Z4	−9.4	−123	990			
Mean		**−9.4 ± 0.2**	**−137 ± 8**	**1,115 ± 76**	**−2.0**	**−734**	**10,570**
Heilongjiang River	L1	−13.9	−34	215			
	L2	−13.4	−28	165			
	L3	−12.6	−39	255			
	L4	−9.2	−110	865			
	SHJ	−8.7	−58	410			
	WSLJ	−9.9	−34	215			
Mean		**−11.3 ± 2.0**	**−51 ± 28**	**354 ± 241**			

Note: space left blanks are not measured. DIC, dissolved inorganic carbon; PIC, particulate inorganic carbon; PY, Poyang Lake; SHJ, Songhuajiang; WSLJ, Wusulijiang; WWT, White-Water Terrace.

high DIC concentrations in the headwater and upper stream of the Yangtze River and the middle stream of the Pearl River could be controlled largely by the weathering of abundant carbonate rocks as suggested in previous studies (Cai et al., 2008; J. Y. Li & Zhang, 2005; Z. L. Wang et al., 2007; Zhang et al., 1995a 1995b). L. J. Zhang et al. (2014) reported that the upper stream of the Yangtze River is the major source of DIC and contributes 47%–61% of the overall riverine DIC flux in the lower reach of the river. As strong evidence, the DIC concentration measured in the WWT carbonate dissolution reference site of this study was 16,198 μM, which was 7.5 times higher than the average riverine DIC concentration. In the lower reach of the Yangtze River, many freshwater lakes that contain low DIC concentrations, such as Poyang (PY), could supply water to the river during the rainy season and dilute the DIC in the main river stream (L. J. Zhang et al., 2014). A recent study by Duvert et al. (2019) addressed the importance of groundwater input of DIC in streams, which could also be an important factor contributing to the DIC contents of the lower reach of the river; however, data have not been reported on this subject in these rivers. In contrast, the Yellow River originates in the same Qinghai-Tibetan Plateau as the Yangtze River. Although the average water discharge rate (29 km^3 $year^{-1}$) of the Yellow River is 30 and 10 times lower than that of the Yangtze and Pearl rivers, respectively, DIC concentration is the highest among the four rivers and remains relatively constant along the entire river (Figure 2a). As reviewed by Cai et al. (2008), the carbonate coverage in the Yellow River drainage basin is relatively low (~7%) and the water evaporation rate (1,100 mm $year^{-1}$) is usually higher than the precipitation rate (476 mm $year^{-1}$) in most of the basin area in summer and fall (J. S. Chen et al., 2006), which often results in high DIC concentrations in the river. The DIC concentration in the Heilongjiang River was the lowest among the four rivers, especially in its main stream (~280 μM) despite its high flow rate. Such findings are similar to that for the Amazon River with the highest discharge rate (6,642 km^3 $year^{-1}$) but much lower DIC concentrations (Figure 4a), suggesting difference sources and influences on the riverine DIC compared with that in the Yangtze, Yellow, and Pearl rivers. We found that the dissolved organic carbon (DOC) concentrations in the Heilongjiang River were much

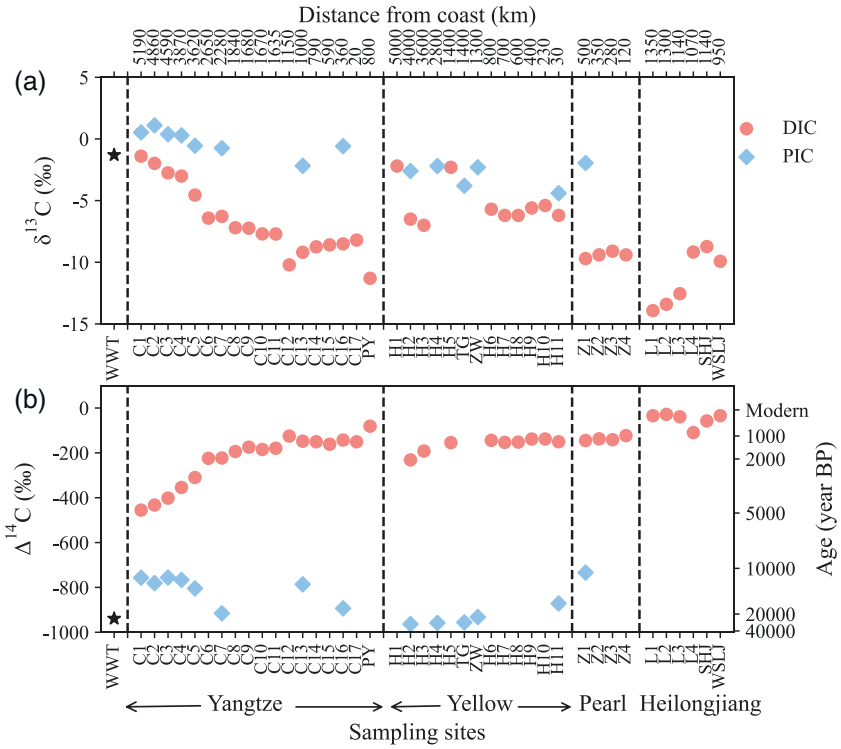

Figure 3. Values of (a) $\delta^{13}C$ and (b) $\Delta^{14}C$ and calculated ^{14}C ages for DIC and PIC in the four rivers. The distance is measured from the river mouth. DIC, dissolved inorganic carbon; PIC, particulate inorganic carbon.

higher (~1,000 μM) than those in the other three rivers (~160 μM; Qi, 2019) and the DOC concentrations exceed the DIC concentrations, which is similar to that in the Amazon River (Mayorga et al., 2005; Richey et al., 1990). We expect that OM respiration could play a major role in affecting the DIC in the Heilongjiang River, which was similar to the case of the Amazon River (Mayorga et al., 2005; Richey et al., 1990). This finding is supported by our isotopic data as discussed in Section 4.3.

Compared with the 12 largest rivers in the world (Figure 4b), the oversaturated pCO_2 in the four large Chinese rivers suggests that these rivers could also be significant sources of CO_2 outgassing to the atmosphere, which is also observed in other large rivers, such as the Amazon and Mississippi (Butman and Raymond, 2011; Reiman and Xu, 2019; Richey, 2004). The pCO_2 in river systems could be controlled largely by an influx of soil CO_2 and in situ respiration of OM (Richey, 2004). The results of our study are also consistent with previous studies conducted for the Yangtze, Yellow and Pearl rivers in which degassing of CO_2 was found to be common, especially in the lower reaches and estuaries of the rivers (Cai et al., 2008; C. T. A. Chen et al., 2008; L. J. Zhang et al., 2014).

4.2. Correlation of DIC with Major Ions

As the major ions produced from rock dissolution during chemical weathering, Ca^{2+} and Mg^{2+} present distributions in the rivers that are positively correlated with DIC as plotted in Figure 5. In the Yangtze and Pearl rivers, a good correlation between the concentrations of HCO_3^- and the ions (Ca^{2+} and Mg^{2+}) was found in our study ($R^2 = 0.86$, $p < 0.001$) and previous studies ($R^2 = 0.76$, $p < 0.001$; $R^2 = 0.85$, $p < 0.001$). Concentrations of HCO_3^- increased linearly with increases in the concentrations of (Ca^{2+} and Mg^{2+}) in the rivers (Figure 5a and 5c). The load of Ca^{2+} was higher than that of Mg^{2+} in both rivers. These similar distribution patterns suggest that the chemical weathering of carbonate rocks along the river basins is likely an important factor influencing the DIC concentration in the Yangtze and Pearl rivers (Cai et al., 2008; L. J. Zhang et al., 2014). In comparison, the concentrations of Mg^{2+} at most sampling sites exceeded those of Ca^{2+} in the Yellow River. A high Mg^{2+} concentration might suggest that the chemical weathering of silicate rocks is higher than that of carbonate rocks along the Yellow River basin considering that the carbonate coverage in the Yellow River drainage basin is relatively low (~7%) (Cai et al., 2008; J. S. Chen et al., 2005; Zhang et al., 1995a 1995b). As

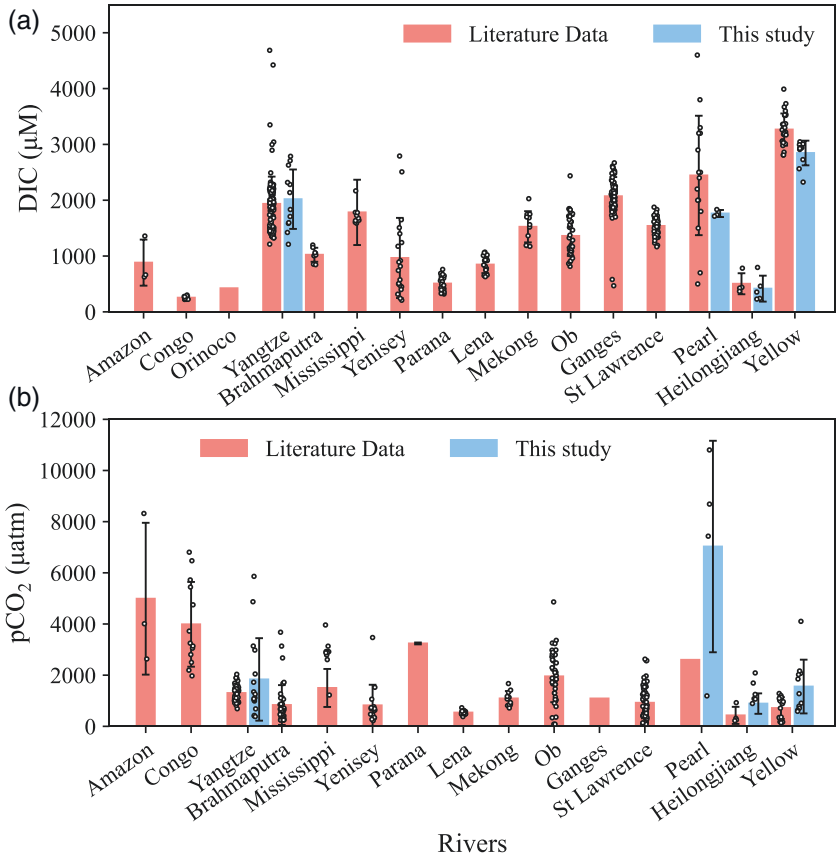

Figure 4. Comparison of (a) DIC and (b) pCO_2 in the four rivers with the 12 largest rivers in the world. The DIC literature data sources: Amazon River ($n = 3$, Mayorga et al., 2005); Congo River ($n = 13$, Z. A. Wang et al., 2013); Yangtze River ($n = 136$, L. J. Zhang et al., 2014; Wu et al., 2008a 2008b); Brahmaputra River ($n = 8$, Singh et al., 2005); Mississippi River ($n = 9$, Reiman & Xu, 2019); Yenisey River ($n = 20$, Prokushkin et al., 2011); Parana River ($n = 25$, Villar & Bonetto, 2000); Lena River ($n = 22$, Semiletov et al., 2011); Mekong River ($n = 11$, S. Li et al., 2013); Ob River ($n = 43$, Pipko et al., 2019); Ganges River ($n = 77$, Chakrapani & Veizer, 2005; Samanta et al., 2015); St Lawrence River ($n = 67$, Hélie et al., 2002); Pearl River ($n = 16$, Z. H. Liu et al. 2017); Heilongjiang River ($n = 4$, Moon et al., 2009); Yellow River ($n = 29$, L. Wang et al., 2016). The pCO_2 literature data sources: Amazon River ($n = 3$, Mayorga et al., 2005); Congo River (n = 13, Z. A. Wang et al., 2013); Yangtze River ($n = 50$, Hartmann et al., 2019); Brahmaputra River ($n = 39$, Hartmann et al., 2019); Mississippi River ($n = 9$, Reiman & Xu, 2019); Yenisey River ($n = 15$, Hartmann et al., 2019); Parana River (average value, S. Li et al., 2013); Lena River ($n = 22$, Semiletov et al., 2011); Mekong River ($n = 11$, S. Li et al., 2013); Ob River ($n = 39$, Pipko et al., 2019); Ganges River (average value, S. Li et al., 2013); St Lawrence River ($n = 67$, Hélie et al., 2002); Pearl River (average value, S. Li et al., 2013); Heilongjiang River ($n = 4$, Hartmann et al., 2019); and Yellow River ($n = 18$, Hartmann et al., 2019). DIC, dissolved inorganic carbon; pCO_2, partial pressure of CO_2.

shown in Figure 5b, the concentrations of HCO_3^- versus (Ca^{2+} and Mg^{2+}) for the Yellow River are weakly correlated ($R^2 = 0.25$, $p < 0.001$ and $R^2 = 0.14$, $p = 0.25$), suggesting that the DIC concentration and distribution in the Yellow River are unlikely to be controlled by carbonate weathering. Among the four rivers we studied, the concentrations of Ca^{2+} and Mg^{2+} in the Heilongjiang River were the lowest. Despite the low concentrations of both DIC and ions in the Heilongjiang River, the concentrations of HCO_3^- versus Ca^{2+} and Mg^{2+} showed strong correlations in our study ($R^2 = 0.98$, $p < 0.001$) and previous studies ($R^2 = 0.80$, $p < 0.001$; Figure 5d). These differences suggest that carbonate weathering could also play a role but is not likely a main contributor to the DIC in the river because the lithology of the Amur River basin is mostly silicate and the cation load in the river has mostly been derived from silicate weathering. Moreover, the silicate weathering rate in the Heilongjiang River is much lower than that of other rivers (Moon et al., 2009).

Based on the variable correlations between the concentrations of HCO_3^- and the ions in these rivers, our study suggests that quantitative estimation of the riverine DIC from the contributions of chemical weather-

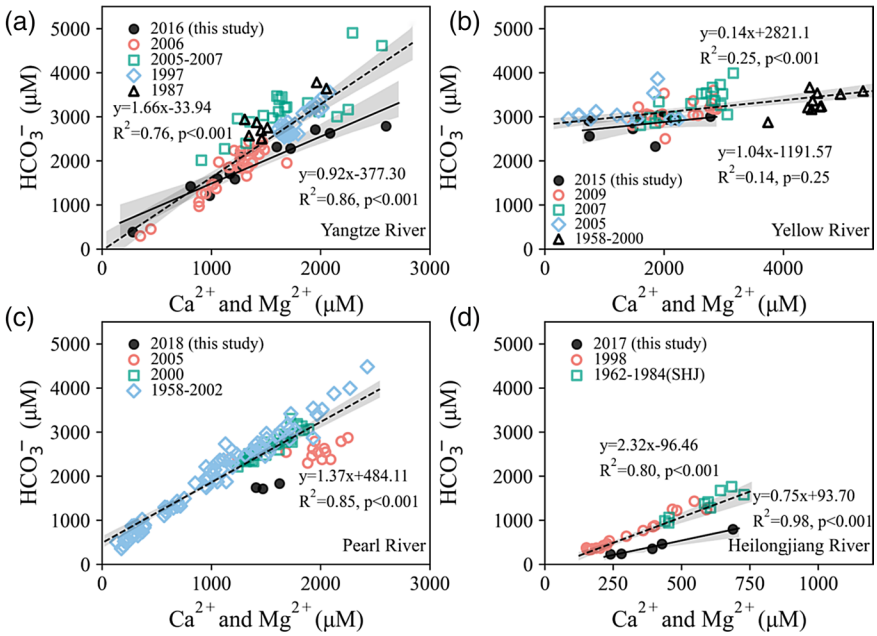

Figure 5. Plots of HCO_3^- versus (Ca^{2+} + Mg^{2+}) concentrations for the four rivers. The solid lines represent the linear relationship of this study, and the dashed lines represent the linear relationship of previous studies. The gray areas show the 95% confidence interval of the linear regression. For the Yangtze River: data for 1987 and 2005–2007 are from Wu et al. (2008a 2008b); data for 1997 are from Z. L. Wang et al. (2007); data for 2006 are from Chetelat et al. (2008). For the Yellow River: data for 1958–2000 are from J. S. Chen et al. (2005); data for 2005 are from Wu et al. (2008) and Z. L. Wang et al. (2007); data for 2007 and 2009 are from Wang et al. (2016). For the Pearl River: data for 2005 are from B. Wang et al. (2012); data for 2000 are from Xu and Liu (2007, 2010); and data for 1958–2002 are from S. R. Zhang et al. (2007). For the Heilongjiang River: data for 1998 are from Moon et al. (2009), and data for 1962–1984 are from Cao et al. (2014).

ing of carbonate and silicate rocks is difficult and limited. This is due to many facts such as the uncertainty of the lithogenic coverage, variable climate, precipitation and evaporation, and variable river flow rates. All these could affect the chemical weathering rate and dissolution dynamic of the ions in rivers (Gaillardet et al., 1999; Goldsmith et al., 2010), thus, resulting in uncertainties of DIC sources in some large rivers in the world as previously reported (Cai et al., 2008; Chetelat et al., 2008; Gaillardet et al., 1999; Moon et al., 2014). These differences can be better distinguished by the carbon isotopic evidence for DIC in rivers.

4.3. Characteristics of DIC Isotopes and Lithology in the Rivers

As discussed above, the DIC in the four rivers was derived from different sources and the carbon isotopic values should reflect the source end-member signatures. The DIC $\delta^{13}C$ values were controlled by the isotopic fractionation and mixing processes of each source end member, such as the consumption of atmospheric CO_2 during chemical weathering of rocks and respiration of OM. In contrast, the $\Delta^{14}C$ values reflect not only the sources but also the ^{14}C age of the source carbon, thus providing more reliable information combined with $\delta^{13}C$ on the origin and cycling of riverine DIC (Marwick et al., 2015; Mayorga et al., 2005; Raymond et al., 2013; X. C. Wang et al., 2016; Zeng & Masiello, 2010).

For the four studied rivers, a very strong correlation occurred between the DIC $\delta^{13}C$ and $\Delta^{14}C$ values ($R^2 = 0.91$, $p < 0.001$) except for the sites in the middle and lower reaches of the Yellow River (Figure 6a). DIC with enriched $\delta^{13}C$ had lower $\Delta^{14}C$ values and old ^{14}C ages, which is also the case in the headwater of the Yangtze River. DIC with more depleted $\delta^{13}C$ had high $\Delta^{14}C$ values with modern ^{14}C ages as observed in the lower reach of the Yangtze River and Heilongjiang River (Figure 6a). The high $\delta^{13}C$ values of DIC (−1.3‰) in the carbonate dissolution reference site WWT and PIC in the rivers (−0.2‰–2.0‰), which were similar to the $\delta^{13}C$ values of carbonate rocks (Hoefs, 2015), provided strong evidence indicating that the DIC in the headwater of the Yangtze River was mainly derived from the dissolution of carbonate rocks during chemical weathering. Moreover, the DIC could have been

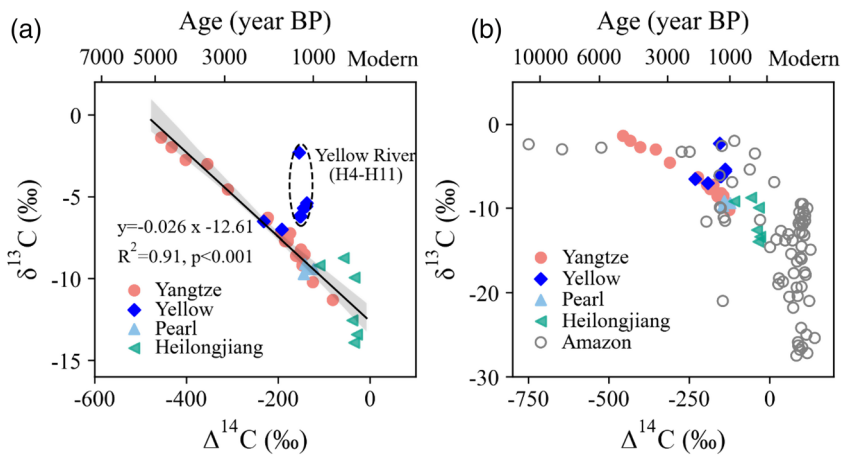

Figure 6. Plots of the measured DIC values of $\delta^{13}C$ versus $\Delta^{14}C$ for the four rivers in China. The solid line represents the linear relationship of the data ($R^2 = 0.91$, $p < 0.001$) and the gray area shows the 95% confidence interval of the linear regression. The sites of H4–H11 in the Yellow River were not included. (b) Plots of the measured DIC values of $\delta^{13}C$ versus $\Delta^{14}C$ in the four rivers in China and in the Amazon River for comparison. The data for the Amazon River were cited from Mayorga et al. (2005). DIC, dissolved inorganic carbon.

influenced by gypsum dissolution (Noh et al., 2009). Downriver, increasing amounts of DIC from OM respiration were likely added to the flowing river, resulting in the more depleted $\delta^{13}C$ and relatively modern $\Delta^{14}C$ values of the riverine DIC as suggested in other studies (Mayorga et al., 2005; Raymond et al., 2013; Zeng & Masiello, 2010). It is also possible that the increased degassing of CO_2 in the lower river could cause isotope fractionation of DIC. Without direct isotope measurements, however, we are not able to quantify the influence of these processes.

The isotopic signatures of DIC in the Yellow River showed obvious differences relative to those of the Yangtze and Pearl rivers (Figure 6a). The DIC isotope values collected in the two upstream sites (H2, H3) fell on the regression line, although DIC collected in the middle and lower reaches of the river (sites H4 to H11) all had similar $\Delta^{14}C$ values (−146 ± 7‰) but was more enriched in $\delta^{13}C$ values than the regression line value (Figure 6a). As discussed above, this finding could suggest that in the middle and lower reaches of the Yellow River, processes other than the weathering of carbonate rocks and OM respiration could play more important roles in controlling the distribution of DIC. In our previous study on DIC in the Yellow River Estuary using carbon isotope (^{13}C and ^{14}C) measurements, we estimated that silicate rock weathering, which consumes atmospheric CO_2, was a major source of DIC in the lower river, thus contributing 73.4 ± 3.0% of the DIC, whereas carbonate dissolution had a less important effect (Wang et al., 2016). The $\Delta^{14}C$ values of the DIC and PIC also distinguished that these two forms of IC in the Yangtze, Yellow, and Pearl rivers were derived from different sources.

There are very limited data of DIC $\delta^{13}C$ and $\Delta^{14}C$ reported for the entire large river basin in the world. In Figure 6b, we compared the DIC $\delta^{13}C$ versus $\Delta^{14}C$ values in the four large rivers in China with the Amazon River reported by Mayorga et al. (2005). The correlation clearly demonstrates the two end member sources of riverine DIC: one with very low $\Delta^{14}C$ (old ^{14}C ages) and high $\delta^{13}C$ values and one with high $\Delta^{14}C$ (modern ^{14}C ages) and low $\delta^{13}C$ values (Figure 6b). For the headwater and upper stream of the Amazon River in the high mountain region, the riverine DIC had very old ^{14}C ages and high $\delta^{13}C$ values as influenced mainly by the carbonate dissolution during weathering, like the case as we found for the Yangtze River. In the middle and low reaches of the Amazon River, it appears that more and more DIC derived from the OM respiration was added to the river, resulting in modern ^{14}C ages and low $\delta^{13}C$ values (Mayorga et al., 2005). These results suggest that the combined carbon isotopic approach can be applied more properly for identification of DIC sources in large rivers with different drainage basins.

To further examine the correlations of DIC isotopes and the ions (Ca^{2+} and Mg^{2+}) produced mainly from the chemical weathering of carbonate and silicate rocks in the rivers, we plotted the DIC $\delta^{13}C$ and $\Delta^{14}C$ values versus $(Ca^{2+} + Mg^{2+})_{sil+carb}$ concentrations, which are the corrected concentrations by subtracting the ions ($Ca^{2+} + Mg^{2+}$) contributed from evaporated rocks from the measured total ion concentrations as described in the caption of Figure 7. A strong correlation between the DIC $\delta^{13}C$ and $\Delta^{14}C$ values and ($Ca^{2+} + Mg^{2+}$)

$_{sil+carb}$ in the Yangtze River can be observed (Figure 7a and 7c). The DIC $\delta^{13}C$ values increased linearly with increasing $(Ca^{2+} + Mg^{2+})_{sil+carb}$ load ($R^2 = 0.78$, $p < 0.001$), and the DIC $\Delta^{14}C$ values decreased linearly with the increase in $(Ca^{2+} + Mg^{2+})_{sil+carb}$ load ($R^2 = 0.82$, $p < 0.001$). These strong isotope and lithological correlations support our above discussion that the DIC in the Yangtze River headwater was derived largely from the carbonate rock weathering and its isotope signatures were diluted with DIC from OM respiration and atmospheric CO_2 consumed by silicate weathering downstream. In contrast, a correlation between the DIC $\delta^{13}C$ values and $(Ca^{2+} + Mg^{2+})_{sil+carb}$ was not seen (Figure 7c). Moreover, a weak opposite correlation was observed, showing that the DIC $\Delta^{14}C$ values slightly increased as the ion concentration increased in the Yellow River (Figure 7d), which supports the conclusion that carbonate rock weathering is not likely the major process contributing DIC in the middle and lower reaches of the Yellow River (Wang et al., 2016). For the Pearl and Heilongjiang rivers, such correlations were not found due to the limited samples.

We also observed good correlations between the DIC isotope values and the concentrations of $[Si]/[HCO_3^-]$ in the Yangtze River as shown also in Figure 7. The DIC $\delta^{13}C$ values decreased linearly with increasing $[Si]/[HCO_3^-]$ load (Figure 7e, $R^2 = 0.70$, $p < 0.001$), and the DIC $\Delta^{14}C$ values increased with increasing $[Si]/[HCO_3^-]$ load (Figure 7g, $R^2 = 0.93$, $p < 0.001$) in the Yangtze River. These strong correlations again suggest that chemical weathering of silicate rocks could also play an important role in controlling the riverine DIC. The weathering of silicate rocks consumes both atmospheric and soil CO_2. The soil CO_2 is derived mainly from soil OM respiration; thus, the soil CO_2 $\delta^{13}C$ values should be more depleted than the atmospheric CO_2 $\delta^{13}C$ (−6.3‰–0‰; Ishikawa et al., 2015; Levin et al., 2010). In the middle and lower reaches of the Yangtze River, in addition to OM respiration, the weathering of silicate rocks increased and consumed more soil CO_2 than atmospheric CO_2, thus contributing more depleted $\delta^{13}C$ and modern $\Delta^{14}C$ to the riverine DIC. In comparison, these trends were not observed in the Yellow River largely due to the relative stable low concentrations of Si and less variable isotope values of DIC (Figure 7f and 7h).

4.4. Quantification of the Potential Sources of DIC in Rivers

The potential sources of riverine DIC depend largely on the environmental and geological setting of the drainage basin of each river. Here, we applied dual isotopes and the MixSIAR model to quantitatively calculate the contribution of the potential sources to DIC in each river. As described in Section 2.5 and plotted in Figure 8, the four potential sources were as follows: (1) DIC produced from the chemical weathering of rocks consuming atmospheric CO_2, (2) DIC produced from the chemical weathering of rocks consuming soil CO_2, (3) carbonate dissolution to DIC during weathering, and (4) DIC produced from OM respiration in the river. The results calculated based on the isotope values for each potential source (Table 2) are shown in Figure 9. Clearly, in the headwater of the Yangtze River (C1–C5), the weathering of carbonate rocks consuming atmospheric CO_2 and the resulting carbonate dissolution were the main sources and contributed 95 ± 5% of the riverine DIC. This contribution is largely related to the geological environment of the Qinghai-Tibetan Plateau, which has abundant carbonate and a thin layer of soil coverage; thus, the weathering of carbonate rocks mainly consumed atmospheric CO_2 (S. L. Li et al., 2014). This finding is also consistent with other studies conducted in the headwater of the Yangtze River (J. Y. Li & Zhang, 2005; S. Y. Li et al., 2011; Noh et al., 2009; Z. L. Wang et al., 2007; Zhang et al., 1995a 1995b). As the Yangtze River flows down, contributions to DIC from the carbonate dissolution decreased and the consumption of atmospheric and soil CO_2 via silicate rock weathering increased in the river (Figure 9a). In the middle and lower reaches of the Yangtze River, the weathering of silicate rocks contributed 62 ± 25% of the riverine DIC, whereas carbonate weathering contributed 33 ± 6% and OM respiration contributed <6%. For soil CO_2, approximately 50% was derived from the respiration of recently fixed OM and 50% was derived from preaged soil OM (Figure 9a).

Compared with the Yangtze River, the contributions to DIC from the weathering of carbonate rocks, weathering of silicate rocks and OM respiration were 42 ± 5%, 55 ± 17%, and 3 ± 3% in the Yellow River, respectively (Figure 9a). These values are consistent with the results reported by Wang et al. (2016), indicating that the consumption of atmospheric and soil CO_2 during silicate rock weathering is an important source of DIC in the Yellow River. Silicate weathering contributed 47 ± 22%, 61 ± 15%, and 61 ± 20% and carbonate weathering contributed 50 ± 7%, 38 ± 5%, and 37 ± 4% of the riverine DIC in the upper, middle, and lower reaches of the Yellow River, respectively. OM respiration had much less of an effect (<3%) on the river DIC.

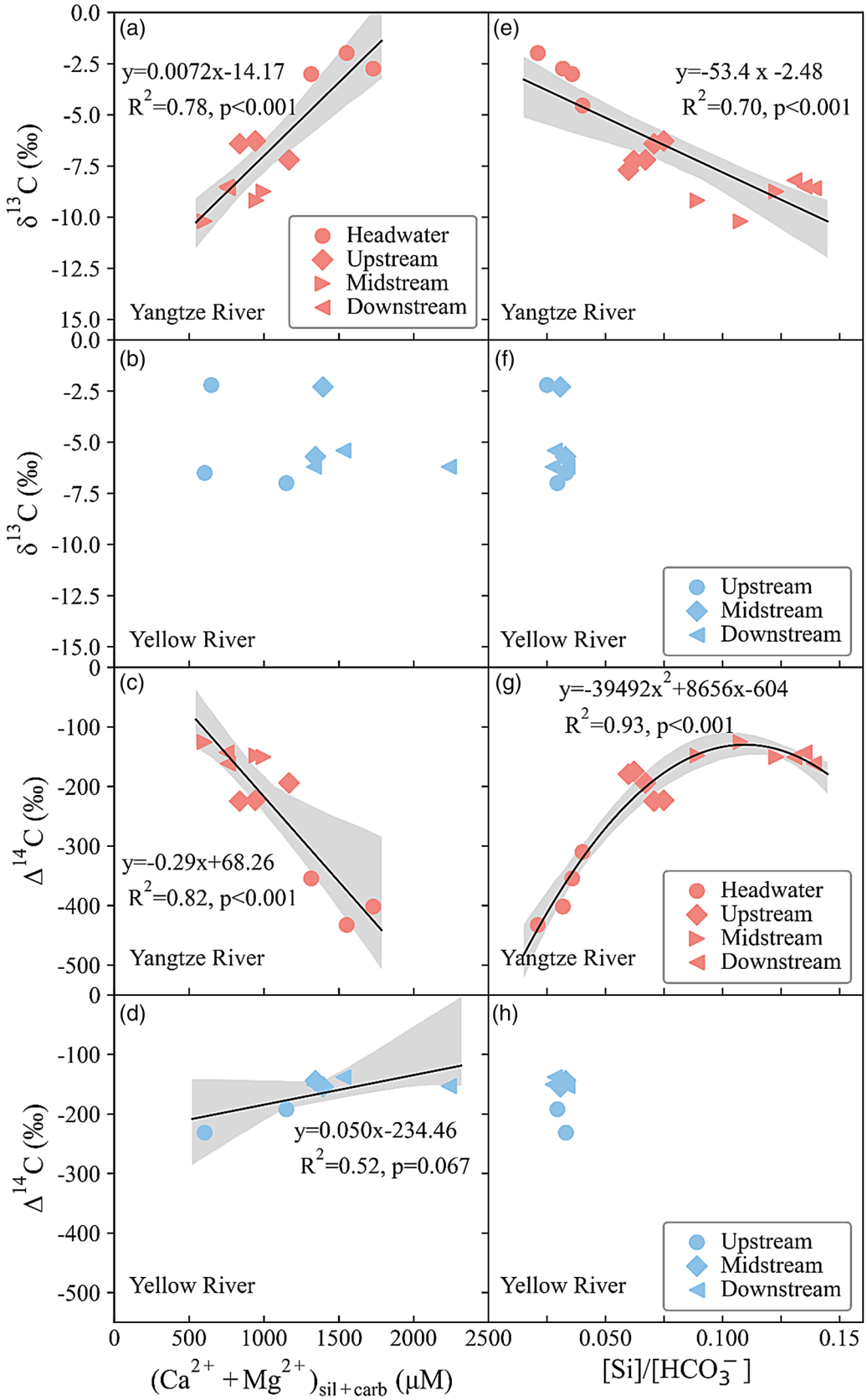
(a)
y=0.0072x-14.17
R2=0.78, p<0.001
Yangtze River
Headwater
Upstream
Midstream
Downstream
(e)
y=-53.4 x -2.48
R2=0.70, p<0.001
Yangtze River
(b)
Yellow River
(f)
Yellow River
Upstream
Midstream
Downstream
(c)
y=-0.29x+68.26
R2=0.82, p<0.001
Yangtze River
(g)
y=-39492x2+8656x-604
R2=0.93, p<0.001
Yangtze River
Headwater
Upstream
Midstream
Downstream
(d)
y=0.050x-234.46
R2=0.52, p=0.067
Yellow River
(h)
Yellow River
Upstream
Midstream
Downstream
δ13C (‰)
Δ14C (‰)
(Ca2+ +Mg2+)sil+carb (μM)
[Si]/[HCO3−]

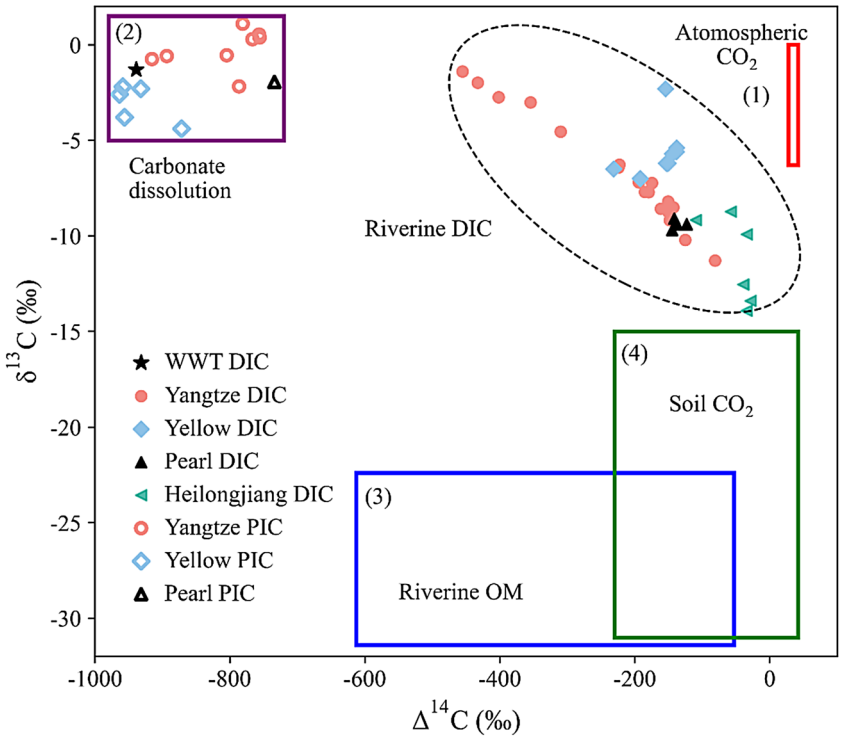

Figure 8. Carbon isotopic ($\delta^{13}C$ vs. $\Delta^{14}C$) values of the potential four sources contributing to the DIC in the four rivers. The potential sources are (1) atmospheric CO_2, (2) soil CO_2, (3) carbonate dissolution and (4) riverine OM respiration. The isotopic values for each source are listed in Table 2.

The DIC in the Pearl River appeared to have similar sources as the DIC in the middle and lower reaches of the Yangtze River, with 61 ± 20% DIC from silicate weathering consuming atmospheric and soil CO_2, 30 ± 4% DIC from carbonate weathering and 9 ± 6% DIC from OM respiration. In the Heilongjiang River, silicate weathering was the major source of DIC, contributing 83 ± 29% of DIC, followed by OM respiration, which contributed 13 ± 10% (Figure 9b). The large calculated contribution of DIC from the atmospheric CO_2 and OM respiration in the Heilongjiang River is well supported by the younger DIC ^{14}C ages (354 ± 241 years BP) relative to that in the other three rivers (1,115–2,189 years BP).

5. Conclusions

This study investigated DIC concentrations and carbon isotopes and revealed the different sources and cycling time scales of DIC in the four largest rivers in China. The following conclusions were drawn from the results.

Figure 7. Plots of the (a) measured DIC values of $\delta^{13}C$ versus concentrations of $(Ca^{2+} + Mg^{2+})_{sil+carb}$ in the Yangtze River; (b) measured DIC values of $\Delta^{14}C$ versus concentrations of $(Ca^{2+} + Mg^{2+})_{sil+carb}$ in the Yangtze River; (c) measured DIC values of $\delta^{13}C$ versus concentrations of $(Ca^{2+} + Mg^{2+})_{sil+carb}$ in the Yellow River; (d) measured DIC values of $\Delta^{14}C$ versus concentrations of $(Ca^{2+} + Mg^{2+})_{sil+carb}$ in the Yellow River; (d) measured DIC values of $\delta^{13}C$ versus concentration ratio of $[Si]/[HCO_3^-]$ in the Yangtze River; (e) measured DIC values of $\Delta^{14}C$ versus concentration ratio of $[Si]/[HCO_3^-]$ in the Yangtze River; (f) measured DIC values of $\delta^{13}C$ versus concentration ratio of $[Si]/[HCO_3^-]$ in the Yellow River; and (h) measured DIC values of $\Delta^{14}C$ versus concentration ratio of $[Si]/[HCO_3^-]$ in the Yellow River. The lines are the linear regression fit to the data. The gray areas show the 95% confidence interval of the linear regression. We used data on riverine ions from the literature to calculate the ratio of silicate and carbonate rocks contributions ($R_{sil+carb}$) to $(Ca^{2+} + Mg^{2+})$. We used SO_4^{2-} as the evaporite contribution of $(Ca^{2+} + Mg^{2+})$ to correct $(Ca^{2+} + Mg^{2+})$. Then, $(Ca^{2+} + Mg^{2+})_{sil+carb}$ can be calculated as follows: $(Ca^{2+} + Mg^{2+})_{sil+carb} = (Ca^{2+} + Mg^{2+}) \times R_{sil+carb}$. The ratio of $[Si]/[HCO_3^-]$ was calculated based on data from previous studies. The data for the Yangtze River were from Wu et al. (2008a 2008b) and Chetelat et al. (2008); and data for the Yellow River were from L. Wang et al. (2016). DIC, dissolved inorganic carbon.

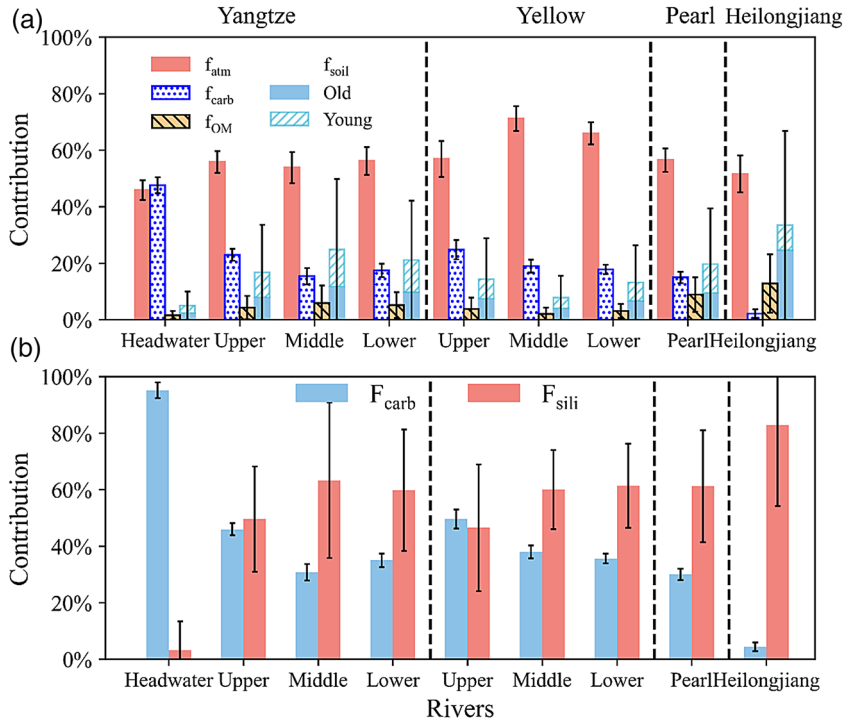

Figure 9. Plots of (a) the calculated mean contributions of the potential four sources to riverine DIC in the four rivers in China. For the soil CO_2, it was divided to two fractions of old and young CO_2 based on the ^{14}C ages; and (b) the calculated mean contributions of the carbonate weathering and silicate weathering to riverine DIC in the four rivers. The error bars represent the ranges of the 95% credible intervals. DIC, dissolved inorganic carbon.

1. The DIC concentrations showed large variations in the four rivers. The Yangtze (2,167 ± 416 μM), Yellow (2,941 ± 206 μM), and Pearl (1,974 ± 268 μM) rivers carried high DIC concentrations, and the Heilongjiang River carried much lower DIC concentrations (448 ± 204 μM). In the Yangtze River, the DIC concentration was high in the headwater and decreased rapidly downstream. In the Yellow River, high DIC was distributed along the whole river. The DIC fluxes in the Yangtze, Pearl, and Yellow rivers were among the top 25 values for the largest rivers of the world.
2. The Yangtze, Yellow, and Pearl Rivers all transported millennium-aged DIC. The ^{14}C ages of the DIC were the oldest (3,950 ± 689 years) in the headwater of the Yangtze River. Furthermore, the Heilongjiang River carried much younger (354 ± 241 years) DIC than the other three rivers. The variable DIC ^{14}C ages and $\delta^{13}C$ values indicate that the riverine DIC was produced by different sources and largely controlled by the environmental and geological setting of the drainage basin of each river. The linear correlation between the DIC isotope values and major lithological ions (Ca^{2+} and Mg^{2+}) suggests that chemical weathering played an important role in controlling the production and distribution of DIC in the Yangtze River. The old DIC transported by the Yangtze, Yellow, and Pearl rivers could have an important influence on carbon cycling and ecosystems in estuaries and coastal waters.
3. Using dual isotopes and the MixSIAR model, we calculated that the weathering of carbonate rocks contributed 95 ± 5% of riverine DIC in the headwater of the Yangtze River and the consumption of atmospheric and soil CO_2 during silicate rock weathering and OM respiration contributed 65 ± 25% and 6 ± 6% of the riverine DIC in the middle and lower reaches of the river, respectively. For the Yellow River, the weathering of carbonate rocks and silicate rocks and OM respiration contributed 42 ± 5%, 55 ± 17%, and 3 ± 3% of the riverine DIC, respectively. Silicate rock weathering appeared to be a major source of DIC in the Yellow River. For the Pearl River, 61 ± 20% of the DIC was from silicate weathering, 9 ± 6% was from OM respiration and 30 ± 4% was from carbonate weathering. In the Heilongjiang River, silicate weathering and OM respiration were the major sources of DIC, and they together contributed 96 ± 40% of the DIC in the river.

Conflict of Interest

The authors declare no conflicts of interest relevant to this study.

Data Availability Statement

Data from all chemical and isotopic analyses of this study are publicly available at figshare.com (via https://doi.org/10.6084/m9.figshare.12416081).

Acknowledgments
The authors thank the members of our laboratory for helping with the sample collection and processing and chemical analyses. The authors give special thanks to the staff of NOSAMS at WHOI and CIGG at QNLM for providing high-precision isotope measurements of the samples. The authors thank the editor and two anonymous reviewers for their comments, which have improved the quality of the manuscript significantly. This study was financially supported by the National Natural Science Foundation of China (Grants # 41776082, 91858210, and 41476057).

References

Amiotte Suchet, P., & Probst, J. L. (1995). A global model for present-day atmospheric/soil CO_2 consumption by chemical erosion of continental rocks (GEM-CO_2). *Tellus B: Chemical and Physical Meteorology*, *47*, 273–280. https://doi.org/10.1034/j.1600-0889.47.issue1.23.x

Bauer, J. E., Cai, W.-J., Raymond, P. A., Bianchi, T. S., Hopkinson, C. S., & Regnier, P. A. G. (2013). The changing carbon cycle of the coastal ocean. *Nature*, *504*, 61–70. https://doi.org/10.1038/nature12857

Beaulieu, E., Goddéris, Y., Donnadieu, Y., Labat, D., & Roelandt, C. (2012). High sensitivity of the continental-weathering carbon dioxide sink to future climate change. *Nature Climate Change*, *2*, 346–349. https://doi.org/10.1038/nclimate1419

Berner, R. A., Lasacga, A. C., & Garrels, R. M. (1983). The carbonate-silicate geochemical cycle and its effect on atmospheric carbon dioxide over the past 100 million years. *American Journal of Science*, *283*, 641–683. https://doi.org/10.2475/ajs.283.7.641

Blair, N. E., & Aller, R. C. (2012). The fate of terrestrial organic carbon in the marine environment. *Annual Review of Marine Science*, *4*, 401–423. https://doi.org/10.1146/annurev-marine-120709-142717

Butman, D., & Raymond, P. A. (2011). Significant efflux of carbon dioxide from streams and rivers in the United States. *Nature Geoscience*, *4*, 839–842. https://doi.org/10.1038/ngeo1294

Cai, W.-J. (2011). Estuarine and coastal ocean carbon paradox: CO_2 sinks or sites of terrestrial carbon incineration?. *Annual Review of Marine Science*, *3*, 123–145. https://doi.org/10.1146/annurev-marine-120709-142723

Cai, W.-J., Guo, X. H., Chen, C.-T. A., Dai, M. H., Zhang, L. J., Zhai, W. D., et al. (2008). A comparative overview of weathering intensity and HCO_3^- flux in the world's major rivers with emphasis on the Changjiang, Huanghe, Zhujiang (Pearl) and Mississippi Rivers. *Continental Shelf Research*, *28*, 1538–1549. https://doi.org/10.1016/j.csr.2007.10.014

Cao, Y. J., Tang, C. Y., Song, X. F., & Liu, C. M. (2014). Major ion chemistry, chemical weathering and CO_2 consumption in the Songhua River basin, Northeast China. *Environmental Earth Sciences*, *73*, 7505–7516. https://doi.org/10.1007/s12665-014-3921-2

Chakrapani, G. J., & Veizer, J. (2005). Dissolved inorganic carbon isotopic compositions in the Upstream Ganga river in the Himalayas. *Current Science*, *89*, 553–556.

Chen, J. S., Wang, F. Y., & He, D. W. (2006). Geochemistry of water quality of the Yellow River basin. *Earth Science Frontiers*, *13*, 58–73.

Chen, J. S., Wang, F. Y., Meybeck, M., He, D. W., Xia, X. H., & Zhang, L. T. (2005). Spatial and temporal analysis of water chemistry records (1958–2000) in the Huanghe (Yellow River) basin. *Global Biogeochemical Cycles*, *19*, GB3016. https://doi.org/10.1029/2004GB002325

Chen, J. S., Wang, F. Y., Xia, X. H., & Zhang, L. T. (2002). Major element chemistry of the Changjiang (Yangtze River). *Chemical Geology*, *187*, 231–255. https://doi.org/10.1016/S0009-2541(02)00032-3

Chen, C.-T. A., Zhai, W. D., & Dai, M. H. (2008). Riverine input and air–sea CO_2 exchanges near the Changjiang (Yangtze River) Estuary: Status quo and implication on possible future changes in metabolic status. *Continental Shelf Research*, *28*, 1476–1482.

Chetelat, B., Liu, C. Q., Zhao, Z. Q., Wang, Q. L., Li, S. L., Li, J., & Wang, B. L. (2008). Geochemistry of the dissolved load of the Changjiang Basin rivers: Anthropogenic impacts and chemical weathering. *Geochimica et Cosmochimica Acta*, *72*, 4254–4277.

Cole, J. J., Prairie, Y. T., Caraco, N. F., McDowell, W. H., Tranvik, L. J., Striegl, R. G., et al. (2007). Plumbing the global carbon cycle: Integrating inland waters into the terrestrial carbon budget. *Ecosystems*, *10*, 171–184.

Dosseto, A., Jack Rink, W., & Thompson, J. W. (2015). Chemical Weathering (U-Series). *Encyclopedia of Scientific Dating Methods*, (152–169). Dordrecht: Springer Netherlands.

Duvert, C., Tyler, K. J., Wynn, J. G., Munksgaard, N. C., Bird, M. I., Setterfield, S. A., & Hutley, L. B. (2019). Groundwater-derived DIC and carbonate buffering enhance fluvial CO_2 evasion in two Australian tropical rivers. *Journal of Geophysical Research - Biogeosciences*, *124*(2), 312–327. http://dx.doi.org/10.1029/2018jg004912

Gaillardet, J., Dupre, B., Louvat, P., & Allegre, C. J. (1999). Global silicate weathering and CO_2 consumption rates deduced from the chemistry of large rivers. *Chemical Geology*, *159*, 3–30.

Ge, T. T., Wang, X. C., Zhang, J., Luo, C. L., & Xue, Y. J. (2016). Dissolved inorganic radiocarbon in the Northwest Pacific continental margin. *Radiocarbon*, *58*, 517–529.

Goldsmith, S. T., Carey, A. E., Johnson, B. M., Welch, S. A., Lyons, W. B., McDowell, W. H., & Pigott, J. S. (2010). Stream geochemistry, chemical weathering and CO_2 consumption potential of andesitic terrains, Dominica, Lesser Antilles. *Geochimica et Cosmochimica Acta*, *74*, 85–103.

Gran, G. (1950). Determination of the equivalence point in potentiometric titrations. Part II. *Analyst*, *77*, 945–947.

Hartmann, J., Jansen, N., Dürr, H. H., Kempe, S., & Köhler, P. (2009). Global CO_2-consumption by chemical weathering: What is the contribution of highly active weathering regions?. *Global and Planetary Change*, *69*, 185–194.

Hartmann, J., & Moosdorf, N. (2012). The new global lithological map database GLiM: A representation of rock properties at the Earth surface. *Geochemistry, Geophysics, Geosystems*, *13*(12). http://dx.doi.org/10.1029/2012gc004370

Hartmann, J., Lauerwald, R., & Moosdorf, N. (2019). GLORICH – Global river chemistry database. Supplement to. A brief overview of the GLObal RIver Chemistry database, GLORICH. Procedia Earth and planetary science (Vol. 10, pp. 23–27) 2014. https://doi.org/10.1594/PANGAEA.902360 Available at https://doi.org/10.1016/j.proeps.2014.08.005

Hélie, J.-F., Hillaire-Marcel, C., & Rondeau, B. (2002). Seasonal changes in the sources and fluxes of dissolved inorganic carbon through the St. Lawrence River—Isotopic and chemical constraint. *Chemical Geology*, *186*, 117–138.

Hirshfield, F., Sui, J., & Ginsberg, S.S. (2011). Changes in Sediment Transport of the Yellow River in the Loess Plateau. *Sediment Transport*, (197–214). InTech. https://www.intechopen.com/books/sediment-transport/changes-in-sediment-transport-of-the-yellow-river-in-the-loess-plateau

Hoefs, J. (2015). *Stable isotope geochemistry*. Cham: Springer International Publishing.
Holland, H. D. (1978). *The chemistry of the atmosphere and oceans*. New York, NY: Wiley.
Ishikawa, N. F., Tayasu, I., Yamane, M., Yokoyama, Y., Sakai, S., & Ohkouchi, N. (2015). Sources of dissolved inorganic carbon in two small streams with different bedrock geology: Insights from carbon isotopes. *Radiocarbon*, *57*, 439–448.
Kump, L. R., Brantley, S. L., & Arthur, M. A. (2000). Chemical weathering, atmospheric CO_2, and climate. *Annual Review of Earth and Planetary Sciences*, *28*, 611–667.
Levin, I., Naegler, T., Kromer, B., Diehl, M., Francey, R. J., Gomez-Pelaez, A. J., et al. (2010). Observations and modelling of the global distribution and long-term trend of atmospheric $^{14}CO_2$. *Tellus B: Chemical and Physical Meteorology*, *62*, 26–46.
Lewis, E., Wallace, D., & Allison, L. J. (1998). *Program developed for CO_2 system calculations*. U.S. Department of Energy.
Li, S. L., Chetelat, B., Yue, F. J., Zhao, Z. Q., & Liu, C. Q. (2014). Chemical weathering processes in the Yalong River draining the eastern Tibetan Plateau, China. *Journal of Asian Earth Sciences*, *88*, 74–84.
Li, S., Lu, X. X., & Bush, R. T. (2013). CO_2 partial pressure and CO_2 emission in the Lower Mekong River. *Journal of Hydrology*, *504*, 40–56.
Li, S. Y., Lu, X. X., He, M., Zhou, Y., Bei, R. T., Li, L., & Ziegler, A. D. (2011). Major element chemistry in the upper Yangtze River: A case study of the Longchuanjiang River. *Geomorphology*, *129*, 29–42.
Liu, S., Butman, D. E., & Raymond, P. A. (2020). Evaluating CO_2 calculation error from organic alkalinity and pH measurement error in low ionic strength freshwaters. *Limnology and Oceanography: Methods*, *18*, 606–622. https://doi.org/10.1002/lom3.10388
Liu, W. G., Yang, H., Ning, Y. F., & An, Z. S. (2007). Contribution of inherent organic carbon to the bulk delta $\delta^{13}C$ signal in loess deposits from the arid western Chinese Loess Plateau. *Organic Geochemistry*, *38*, 1571–1579. https://doi.org/10.1016/j.orggeochem.2007.05.004
Liu, Z. Y., Zhang, L. J., Cai, W.-J., Wang, L., Xue, M., & Zhang, X. S. (2014). Removal of dissolved inorganic carbon in the Yellow River Estuary. *Limnology & Oceanography*, *59*, 413–426. https://doi.org/10.4319/lo.2014.59.2.0413
Liu, Z. H., Zhao, M., Sun, H., Yang, R., Chen, B., Yang, M. X., et al. (2017). "Old" carbon entering the South China Sea from the carbonate-rich Pearl River Basin: Coupled action of carbonate weathering and aquatic photosynthesis. *Applied Geochemistry*, *78*, 96–104.
Li, J. Y., & Zhang, J. (2005). Chemical weathering processes and atmospheric CO_2 consumption of Huanghe River and Changjiang River basins. *Chinese Geographical Science*, *15*, 16–21.
Ludwig, W., Probst, J.-L. (1998). River sediment discharge to the oceans; present-day controls and global budgets. *American Journal of Science*, *298*(4), 265–295. http://dx.doi.org/10.2475/ajs.298.4.265
Luo, C. L. (2017). Carbon isotopic (13C, 14C) studies of the sources, seasonal variation and flux of inorganic carbon transported by the Huanghe River (MS Thesis). Ocean University of China.
Marwick, T. R., Tamooh, F., Teodoru, C. R., Borges, A. V., Darchambeau, F., & Bouillon, S. (2015). The age of river-transported carbon: A global perspective. *Global Biogeochemical Cycles*, *29*, 122–137. https://doi.org/10.1002/2014GB004911
Mayorga, E., Aufdenkampe, A. K., Masiello, C. A., Krusche, A. V., Hedges, J. I., Quay, P. D., et al. (2005). Young organic matter as a source of carbon dioxide outgassing from Amazonian rivers. *Nature*, *436*, 538–541.
McNichol, A. P., Jones, G. A., Hutton, D. L., Gagnon, A. R., & Key, R. M. (1994). The rapid preparation of seawater ΣCO_2 for radiocarbon analysis at the National Ocean Sciences Ams Facility. *Radiocarbon*, *36*, 237–246.
Meybeck, M. (1976). Total mineral dissolved transport by world major rivers. *Hydrological Sciences Bulletin*, *21*, 265–284.
Meybeck, M. (1987). Global chemical weathering of surficial rocks estimated from river dissolved loads. *American Journal of Science*, *287*, 401–428.
Meybeck, M. (1993). Riverine transport of atmospheric carbon: Sources, global typology and budget. *Water, Air, and Soil Pollution*, *70*, 443–463.
Millero, F. J. (1979). The thermodynamics of the carbonate system in seawater. *Geochimica et Cosmochimica Acta*, *43*, 1651–1661.
Millero, F. J. (2013). *Chemical oceanography* (4th ed.). New York: CRC Press.
Milliman, J. D., & Meade, R. H. (1983). World-wide delivery of river sediment to the oceans. *The Journal of Geology*, *91*, 1–21.
Ministry of Water Resources of The People's Republic of China. (2018). *Sediment Bulletin of Chinese rivers*. Beijing: China Water & Power Press.
Moon, S., Chamberlain, C. P., & Hilley, G. E. (2014). New estimates of silicate weathering rates and their uncertainties in global rivers. *Geochimica et Cosmochimica Acta*, *134*, 257–274.
Moon, S., Huh, Y., & Zaitsev, A. (2009). Hydrochemistry of the Amur River: Weathering in a Northern Temperate Basin. *Aquatic Geochemistry*, *15*, 497–527.
Noh, H., Huh, Y., Qin, J., & Ellis, A. (2009). Chemical weathering in the Three Rivers region of Eastern Tibet. *Geochimica et Cosmochimica Acta*, *73*, 1857–1877.
Pipko, I. I., Pugach, S. P., Savichev, O. G., Repina, I. A., Shakhova, N. E., Moiseeva, Y. A., et al. (2019). Dynamics of dissolved inorganic carbon and CO_2 fluxes between the water and the atmosphere in the main channel of the Ob River. *Doklady Chemistry*, *484*, 52–57.
Prokushkin, A. S., Pokrovsky, O. S., Shirokova, L. S., Korets, M. A., Viers, J., Prokushkin, S. G., et al. (2011). Sources and the flux pattern of dissolved carbon in rivers of the Yenisey basin draining the Central Siberian Plateau. *Environmental Research Letters*, *6*, 045212.
Qi, Y. Z. (2019). Distribution and carbon isotopic (13C, 14C) studies of organic carbon in the Changjiang River and East China Sea (MS Thesis). Ocean University of China.
R Core Team. (2019). *R: A language and environment for statistical computing*. Vienna: R Foundation for Statistical Computing.
Raymond, P. A., Hartmann, J., Lauerwald, R., Sobek, S., McDonald, C., Hoover, M., et al. (2013). Global carbon dioxide emissions from inland waters. *Nature*, *503*, 355–359.
Raymond, P. A., McClelland, J. W., Holmes, R. M., Zhulidov, A. V., Mull, K., Peterson, B. J., et al. (2007). Flux and age of dissolved organic carbon exported to the Arctic Ocean: A carbon isotopic study of the five largest Arctic rivers. *Global Biogeochemical Cycles*, *21*, GB4011. https://doi.org/10.1029/2007GB002934
Raymo, M. E., & Ruddiman, W. F. (1992). Tectonic forcing of late Cenozoic climate. *Nature*, *359*, 117–122.
Reeder, S. W., Hitchon, B., & Levinson, A. A. (1972). Hydrogeochemistry of the surface waters of the Mackenzie River drainage basin, Canada—I. Factors controlling inorganic composition. *Geochimica et Cosmochimica Acta*, *36*, 825–865.
Regnier, P., Friedlingstein, P., Ciais, P., Mackenzie, F. T., Gruber, N., Janssens, I. A., et al. (2013). Anthropogenic perturbation of the carbon fluxes from land to ocean. *Nature Geoscience*, *6*, 597–607.
Reiman, J. H., & Xu, Y. J. (2019). Dissolved carbon export and CO_2 outgassing from the lower Mississippi River—Implications of future river carbon fluxes. *Journal of Hydrology*, *578*, 124093.
Richey, J. E., Field, C. B., Raupach, M. R., & Ebrary, I. (2004). Pathways of atmospheric CO_2 through fluvial systems. *The Global Carbon Cycle: Integrating Humans, Climate, and The Natural World*, SCOPE, (329–340). Washington: Island Press.
Richey, J. E., Hedges, J. I., Devol, A. H., Quay, P. D., Victoria, R., Martinelli, L., & Forsberg, B. R. (1990). Biogeochemistry of carbon in the Amazon River. *Limnology & Oceanography*, *35*, 352–371.

Richey, J. E., Melack, J. M., Aufdenkampe, A. K., Ballester, V. M., & Hess, L. L. (2002). Outgassing from Amazonian rivers and wetlands as a large tropical source of atmospheric CO_2. *Nature*, *416*, 617–620.

Samanta, S., Dalai, T. K., Pattanaik, J. K., Rai, S. K., & Mazumdar, A. (2015). Dissolved inorganic carbon (DIC) and its $\delta^{13}C$ in the Ganga (Hooghly) River estuary, India: Evidence of DIC generation via organic carbon degradation and carbonate dissolution. *Geochimica et Cosmochimica Acta*, *165*, 226–248.

E. A. G. Schuur, E. Druffel, & S. E. Trumbore (Eds.), (2016). *Radiocarbon and climate change*. Cham: Springer International Publishing.

Semiletov, I. P., Pipko, I. I., Shakhova, N. E., Dudarev, O. V., Pugach, S. P., Charkin, A. N., et al. (2011). Carbon transport by the Lena River from its headwaters to the Arctic Ocean, with emphasis on fluvial input of terrestrial particulate organic carbon vs. carbon transport by coastal erosion. *Biogeosciences*, *8*, 2407–2426.

Singh, S. K., Sarin, M. M., & France-Lanord, C. (2005). Chemical erosion in the eastern Himalaya: Major ion composition of the Brahmaputra and δ13C of dissolved inorganic carbon. *Geochimica et Cosmochimica Acta*, *69*, 3573–3588.

Stets, E. G., Butman, D., McDonald, C. P., Stackpoole, S. M., DeGrandpre, M. D., & Striegl, R. G. (2017). Carbonate buffering and metabolic controls on carbon dioxide in rivers. *Global Biogeochemical Cycles*, *31*, 663–677. https://doi.org/10.1002/2016GB005578

Stock, B. C., & Semmens, B. X. (2016). *Mixsiar GUI user manual. Version 3.1*. Zenodo. Available at https://github.com/brianstock/MixSIAR

Stuiver, M., & Polach, H. A. (1977). Discussion reporting of ^{14}C data. *Radiocarbon*, *19*, 355–363.

Tao, S. Q., Eglinton, T. I., Montluçon, D. B., McIntyre, C., & Zhao, M. X. (2016). Diverse origins and pre-depositional histories of organic matter in contemporary Chinese marginal sea sediments. *Geochimica et Cosmochimica Acta*, *191*, 70–88.

Tu, C. L., Liu, C. Q., Quine, T. A., Jones, M. W., Liu, T. Z., Li, L. B., & Liu, W. J. (2018). Dynamics of soil organic carbon following land-use change: insights from stable C-isotope analysis in black soil of Northeast China. *Acta Geochimica*, *37*, 746–757.

Villar, C. A., & Bonetto, C. (2000). Chemistry and nutrient concentrations of the Lower Parana River and its floodplain marshes during extreme flooding. *Archiv Fur Hydrobiologie*, *148*, 461–479.

Wachniew, P. (2006). Isotopic composition of dissolved inorganic carbon in a large polluted river: The Vistula, Poland. *Chemical Geology*, *233*, 293–308.

Walling, D. E., & Fang, D. (2003). Recent trends in the suspended sediment loads of the world's rivers. *Global and Planetary Change*, *39*, 111–126.

Wang, Z. A., Bienvenu, D. J., Mann, P. J., Hoering, K. A., Poulsen, J. R., Spencer, R. G. M., & Holmes, R. M. (2013). Inorganic carbon speciation and fluxes in the Congo River. *Geophysical Research Letters*, *40*, 511–516. https://doi.org/10.1002/grl.50160

Wang, S., Fu, B. J., Piao, S. L., Lu, Y. H., Ciais, P., Feng, X. M., & Wang, Y. F. (2016). Reduced sediment transport in the Yellow River due to anthropogenic changes. *Nature Geoscience*, *9*, 38–41.

Wang, B., Lee, X.-Q., Yuan, H.-L., Zhou, H., Cheng, H.-G., Cheng, J.-Z., et al. (2012). Distinct patterns of chemical weathering in the drainage basins of the Huanghe and Xijiang River, China: Evidence from chemical and Sr-isotopic compositions. *Journal of Asian Earth Sciences*, *59*, 219–230.

Wang, X. C., Luo, C. L., Ge, T. T., Xu, C. L., & Xue, Y. J. (2016). Controls on the sources and cycling of dissolved inorganic carbon in the Changjiang and Huanghe River estuaries, China: ^{14}C and ^{13}C studies. *Limnology & Oceanography*, *61*, 1358–1374. https://doi.org/10.1002/lno.10301

Wang, L., Zhang, L. J., Cai, W. J., Wang, B. S., & Yu, Z. G. (2016). Consumption of atmospheric CO_2 via chemical weathering in the Yellow River basin: The Qinghai-Tibet Plateau is the main contributor to the high dissolved inorganic carbon in the Yellow River. *Chemical Geology*, *430*, 34–44.

Wang, Z. L., Zhang, J., & Liu, C. Q. (2007). Strontium isotopic compositions of dissolved and suspended loads from the main channel of the Yangtze River. *Chemosphere*, *69*, 1081–1088.

Wu, L. L., Huh, Y., Qin, J. H., Du, G., & van Der Lee, S. (2005). Chemical weathering in the Upper Huang He (Yellow River) draining the eastern Qinghai-Tibet Plateau. *Geochimica et Cosmochimica Acta*, *69*, 5279–5294.

Wu, W. H., Xu, S. J., Yang, J. D., & Yin, H. W. (2008a). Silicate weathering and CO_2 consumption deduced from the seven Chinese rivers originating in the Qinghai-Tibet Plateau. *Chemical Geology*, *249*, 307–320.

Wu, W. H., Yang, J. D., Xu, S. J., & Yin, H. W. (2008b). Geochemistry of the headwaters of the Yangtze River, Tongtian He and Jinsha Jiang: Silicate weathering and CO_2 consumption. *Applied Geochemistry*, *23*, 3712–3727.

Wu, Y., Zhang, J., Liu, S. M., Zhang, Z. F., Yao, Q. Z., Hong, G. H., & Cooper, L. (2007). Sources and distribution of carbon within the Yangtze River system. *Estuarine, Coastal and Shelf Science*, *71*, 13–25.

Q. Q. Xu (Ed.), (2006). *Water conservancy encyclopedia China* (2nd ed.). China Water & Power Press.

Xue, Y. J., Zou, L., Ge, T. T., & Wang, X. C. (2017). Mobilization and export of millennial-aged organic carbon by the Yellow River. *Limnology & Oceanography*, *62*, S95–S111. https://doi.org/10.1002/lno.10579

Xu, Z. F., & Liu, C. Q. (2007). Chemical weathering in the upper reaches of Xijiang River draining the Yunnan–Guizhou Plateau, Southwest China. *Chemical Geology*, *239*, 83–95.

Xu, Z. F., & Liu, C. Q. (2010). Water geochemistry of the Xijiang basin rivers, South China: Chemical weathering and CO_2 consumption. *Applied Geochemistry*, *25*, 1603–1614.

Yu, F. L., Zong, Y. Q., Lloyd, J. M., Huang, G. Q., Leng, M. J., Kendrick, C., et al. (2010). Bulk organic $\delta^{13}C$ and C/N as indicators for sediment sources in the Pearl River delta and estuary, southern China. *Estuarine, Coastal and Shelf Science*, *87*, 618–630.

Zeng, F. W., & Masiello, C. A. (2010). Sources of CO_2 evasion from two subtropical rivers in North America. *Biogeochemistry*, *100*, 211–225.

Zeng, F. W., Masiello, C. A., & Hockaday, W. C. (2011). Controls on the origin and cycling of riverine dissolved inorganic carbon in the Brazos River, Texas. *Biogeochemistry*, *104*, 275–291.

Zhang, J., Huang, W. W., Létolle, R., & Jusserand, C. (1995a). Major element chemistry of the Huanghe (Yellow River), China – Weathering processes and chemical fluxes. *Journal of Hydrology*, *168*, 173–203.

Zhang, S.-R., Lu, X. X., Higgitt, D. L., Chen, C.-T. A., Sun, H.-G., & Han, J.-T. (2007). Water chemistry of the Zhujiang (Pearl River): Natural processes and anthropogenic influences. *Journal of Geophysical Research*, *112*, F01011. https://doi.org/10.1029/2006JF000493

Zhang, J., Quay, P. D., & Wilbur, D. O. (1995b). Carbon isotope fractionation during gas-water exchange and dissolution of CO_2. *Geochimica et Cosmochimica Acta*, *59*, 107–114.

Zhang, L. J., Wang, L., Cai, W. J., Liu, D. M., & Yu, Z. G. (2013). Impact of human activities on organic carbon transport in the Yellow River. *Biogeosciences*, *10*, 2513–2524.

Zhang, L. J., Xue, M., Wang, M., Cai, W.-J., Wang, L., & Yu, Z. G. (2014). The spatiotemporal distribution of dissolved inorganic and organic carbon in the main stem of the Changjiang (Yangtze) River and the effect of the Three Gorges Reservoir. *Journal of Geophysical Research: Biogeosciences*, *119*, 741–757. https://doi.org/10.1002/2012JG002230